PEOPLE'S DEMOCRATIC REPUBLIC OF ALGERIA
Ministry of Higher Education and Scientific Research

UNIVERSITY OF BLIDA 1
Faculty of Technology
Department of Process Engineering

Thesis

In partial fulfillment of the requirements for the degree of

MASTER OF PROCESS ENGINEERING

Specialization: Chemical Engineering

Simulation and analysis of the performance of electrolysers for hydrogen production: influence of operational parameters

Presented by:

DOUKHI Ikbel

OUAISSA Lina

Supervised by:

Dr Mohamed El Moundir Hadji

Prof Mohamed Wahib Naceur

Academic Year: 2024/2025

ملخص:

تُقدم هذه الدراسة إطار محاكاة متكامل يجمع بين نمذجة معالجة المياه باستخدام برنامج WAVE ونموذج كيميائي كهربائي دقيق لمحلل كهربائي يعمل بغشاء تبادل بروتوني (PEM) في برنامج Simulink. وتهدف إلى تقييم تأثير جودة المياه المعالجة من تكوينات التحلية بالتناضح العكسي (RO) والترشيح النانوي (NF) على إنتاج الهيدروجين وكفاءة النظام على المدى الطويل.

تمت دراسة ثلاثة مصادر مائية في الجزائر: مياه البحر، مياه حوض اللياس، ومياه حوض الألبين. أظهرت نتائج WAVE أن الأنظمة الهجينة، خاصةRO/NF90 ، تحقق توازنًا جيدًا بين نقاء المياه واستهلاك الطاقة — على سبيل المثال، وصلت مياه اللياس إلى موصلية كهربائية قدرها 9 ميكروسيمنز/سم باستهلاك طاقة قدره 0.89 ك.و.س/م³.

تم استخدام هذه القيم في نموذج PEM لمحاكاة الكفاءة، إنتاج الغاز، وتدهور الأداء بمرور الوقت. أظهرت النتائج أن مياه اللياس توفر أفضل أداء إجمالي، من حيث النقاء، وتكلفة الطاقة، والاستقرار طويل الأمد.

يساعد هذا النهج على تحسين إنتاج الهيدروجين من خلال الربط بين معالجة المياه وأداء المحلل الكهربائي.

الكلمات المفتاحية:معالجة المياه, لمحلل كهربائي بغشاء تبادل بروتوني, إنتاج الهيدروجين, جودة المياه

Abstract

This study presents an integrated simulation framework combining WAVE-based water treatment modeling with a detailed PEM electrolyzer model in Simulink. It evaluates how water quality from different RO/NF configurations affects hydrogen production and long-term efficiency.

Three Algerian water sources were studied: seawater, Lias, and Albian aquifer water. WAVE results showed that hybrid systems, especially RO/NF90, provide a good balance of purity and energy use—e.g., Lias water reached 9 µS/cm at 0.89 kWh/m³. These values fed into the PEM model, which simulated efficiency, gas output, and degradation over time.

Results showed that Lias water offers the best overall performance, balancing purity, energy cost, and durability. This approach helps optimize hydrogen production by linking water treatment and electrolyzer performance.

Key words: water treatment, (PEM) electrolyzer, hydrogen production, degradation .

Résumé

Cette étude présente un cadre de simulation intégré combinant la modélisation du traitement de l'eau via le logiciel WAVE et un modèle électrochimique détaillé d'un électrolyseur à membrane échangeuse de protons (PEM) développé sous Simulink. Elle vise à évaluer l'impact de la qualité de l'eau traitée à partir de différentes configurations d'osmose inverse (RO) et de nanofiltration (NF) sur la production d'hydrogène et l'efficacité à long terme du système.

Trois sources d'eau en Algérie ont été étudiées : l'eau de mer, l'eau de la nappe du Lias et celle de la nappe de l'Albien. Les résultats issus de WAVE ont montré que les systèmes hybrides, notamment RO/NF90, offrent un bon compromis entre pureté de l'eau et consommation énergétique — par exemple, l'eau du Lias a atteint une conductivité de 9 µS/cm avec une consommation de 0,89 kWh/m³.

Ces valeurs ont été utilisées dans le modèle PEM pour simuler le rendement, la production de gaz et la dégradation des performances dans le temps. Les résultats ont révélé que l’eau du Lias offre la meilleure performance globale en termes de pureté, de coût énergétique et de stabilité à long terme.

Cette approche permet d’optimiser la production d’hydrogène en établissant un lien entre le traitement de l’eau et le comportement de l’électrolyseur.

Mots clés : traitement de l’eau, un électrolyseur (PEM) , production d’hydrogène , degradation , qualité de l’eau

Acknowledgments:

*We extend our profound gratitude to **Allah** for bestowing upon us the courage, strength, and well-being necessary to successfully accomplish this humble undertaking.*

*We would like to express our sincere gratitude to our supervisor, **Mr. Hadji**, for his valuable advice, continuous support, and trust throughout this thesis. His professional guidance and thoughtful feedback greatly contributed to the success of our work.*

*we also extend our thanks to our co-supervisor, **Mr. Naceur Wahib**, for his consistent follow-up, insightful suggestions, and helpful encouragement during each stage of this research.*

Dedication

My deepest thanks go to my parents for their love and endless support, and to my brother Haithem and sister Ibtihel for always being there for me. I am forever grateful for their presence in my life.

My special thanks go to my best friend, Ghadir, for her kindness, support, and for always being by my side through the ups and downs.

I express my heartfelt gratitude to my dear uncle and his family for their unwavering support, kindness, and generosity, which have been invaluable throughout this journey

I would like to express my heartfelt gratitude to my English group, whose unwavering dedication and enthusiasm have greatly enhanced my learning journey. Their support and collaboration have been instrumental in fostering both personal growth and academic development throughout my studies.

Finally, I thank my English teacher, Mr. Bessam Hichem, for helping me improve my language skills and encouraging me during my studies.

I am extremely grateful to my binom Lina, without whom this work would not have been accomplished in this manner.

As well as all those who have helped us, whether directly or indirectly, in our work, may they be thanked here.

DOUKHI Ikbel

Dedication

I dedicate this work with profound gratitude and love:

To my beloved parents, whose sacrifices, unwavering encouragement, and unconditional love have been the foundation of all my achievements.

To my dear grandmother, whose wisdom and heartfelt prayers have always been a source of strength and inspiration.

To my brother Samir, who has always been a role model to me, embodying perseverance, integrity, and relentless hard work. Your example inspires me to strive for excellence in all that I do.

To my cherished sisters, Meriem, Manel, and Lidya, whose love, laughter, and companionship have brought joy and balance to my journey, constantly reminding me of the importance of family and resilience.

To my brother's wife, Zahira, and their wonderful children, Nassim and Eline, whose presence has enriched our family with love, warmth, and unforgettable memories.

To my binom, Ikbal, thank you for your support, kindness, and wonderful collaboration throughout this journey.

This work is a reflection of the love, support, and inspiration I have received from each one of you.

Thank you for being my greatest blessings.

OUAISSA Lina

List of contents

List of Figures

List of Tables

Symboles

A_m	The membrane section area
$A_i\pi_i$	Membrane permeability at 25°C for element i, a function of the average concentrate-side osmotic pressure (gfd/psi)
$\bar{A}\pi$	Average membrane permeability at 25°C: a function of the average concentrate-side osmotic pressure (gfd/psi)
$b_{membrane}$	degradation rate of the membrane
C_t	total thermal capacity
$c_{c,p}$	specific heat
$C_{O2,mem}$	Oxygen concentration
$C_{H2,mem}$	hydrogen concentration
C_{fci}	Average concentrate-side concentration for element i (ppm)
C_{fi}	Feed concentration for element i (ppm)
C_{ci}	Concentration for element i (ppm)
$\bar{C}_{fc}$	Average concentrate-side concentration for the system (ppm)
E	electrical energy consumption
E_{spec}	Specific energy
F	Faraday's constant
F_{H2}	hydrogen flowrate
FF	Membrane fouling factor
I	The current
i	Current density
i_0	Exchange current density
i_{lim}	Limiting current density
k	Empirical coefficient
l_{water}	The thickness of the water layer
l_m	Membrane thickness
$\dot{m}_{H2}$	The mass flow rate of hydrogen

$\dot{m}_{H2O\_reacted}$	The mass flow rate of water
$\dot{m}_{O2}$	The mass flow rate of oxygen
$\dot{m}_{c}$	coolant mass flow rate
M_{H2}	Molar mass of hydrogen
M_{O2}	Molar mass of oxygen
M_{H20}	Molar mass of water
m_j	Molal concentration of j th ion species
$\dot{n}_{H2}$	The molar flow rate of hydrogen
$\dot{n}_{O2}$	The molar flow rate of oxygen
$\dot{n}_{H2O}$	The molar flow rate of water
n_c	the number of electrolytic cells
N_E	Number of element in system
N_V	Number of six-element pressure vessels in system (≈ $N_E/6$)
N_{V1}	Number of pressure vessels in first stage of 2-stage system (≈ 1/3 NV)
N_{V2}	number of pressure vessels in second stage of 2-stage system (≈ $N_V/3$)
N_{VR}	stage ratio (=N_{V1}/N_{V2})
n	Number of elements in system
P_{H2}	Partial pressures of hydrogen
P_{O2}	Partial pressures of oxygen
P_{H2O}	Partial pressures of water vapor
P_{Elec}	the electrical power
P_{fi}	Feed pressure of element i (psi)
P_{pi}	Permeate pressure of element i (psi)
Pf_i	Concentration polarization factor for element i
$\overline{pf}$	Average concentration polarization factor
Q_i	Permeate flow of element i (gpd)
Q	System permeate flow (gpd)
$\bar{Q}_i$	Average element permeate flow (gpd) = Q/NE
$\bar{q}_{fc}$	Arithmetic average concentrate-side flowrate (gpm) [= (1/2)(feed flow + concentrate flow)]
$Q_{generation}$	The transient heat generation
Q_{loss}	The transient heat loss

Q_{cool}	The cooling rate
R	Ideal gas constant
R_t	The total thermal resistance
R_{total}	The total resistance
$R_{membrane}$	The resistance of the membrane
$R_{0_{membrane}}$	The Initial Membrane Strength
R_{water}	The resistance of the water layer
R_{ohm}	The Ohmic resistance
R_i	Salt rejection fraction for element i
$\bar{R}$	Average fractional salt rejection for the system
S_E	Membrane surface area per element (ft^2)
T	Temperature
T_{amb}	The ambient temperature
$T_{c,in}$	The coolant temperature in
$T_{c,out}$	The coolant temperature out
TCF	Temperature correction factor for membrane permeability
V_{tn}	thermoneutral voltage
V_{cell}	cell voltage
V_{rev}	Reversible potential
V_{ohm}	Ohmic overpotential
V_{act}	Activation overpotential
V_{con}	Concentration overpotential
V_0	Standard reversible potential
$V_{con,a}$	The concentration overpotential at the anode side
$V_{con,c}$	The concentration overpotential at the cathode side
Y_i	Recovery fraction for element i
Y	System recovery (expressed as a fraction) = permeate flow/feed flow

Y_L	Limiting (maximum) system recovery (expressed as a fraction)
$\bar{Y}_i$	Average element recovery (expressed as a fraction)
z	Number of electrons per reaction
ρ_{H2}	density of hydrogen
λ_m	Membrane hydration level
σ_m	The conductivity of the membrane
σ_{water}	water conductivity
η	Voltage efficiency
η_F	Faraday's efficiency
$\eta_{\mathrm{Electrical}}$	Electrical efficiency
$\propto$	Charge transfer coefficient
$\propto_a$	The charge transfer coefficient for anodes
$\propto_c$	The charge transfer coefficient for cathodes
ΔP_{fci}	Concentrate-side pressure drop for Element i (psi)
$\Delta\bar{P}_{fc}$	Average concentrate-side system pressure drop (psi)
$\bar{\pi}_i$	Average concentrate-side osmotic pressure (psi)
π_{fi}	Feed osmotic pressure of element i
π_{pi}	Permeate side osmotic pressure of element i
π_f	Treated feed water osmotic pressure (psi)
$\bar{\pi}$	Average concentrate-side osmotic pressure for the system (psi)
$\sum_j$	Summation of all ionic species
$\prod_{i=1}^{n}$:	Multiplication of n terms in a series

Acronyms

AEM	anion-exchange membrane
AWE	alkaline water electrolysis
DC	direct current
HER	hydrogen evolution reaction
ICEs	internal combustion engines
MEA	Membrane Electrode Assembly
NF	Nano filtration
OER	oxygen evolution reaction
PEM	proton-exchange membrane
PEME	Polymer Electrolyte Membrane Electrolysis
PTL	Porous Transport Layer
RO	reverse osmosis
SMR	Steam Methane Reforming
SOEC	solid oxide electrolysis cell
SPE	solid polymer electrolyte
TDS	Total Dissolved Solids

General Introduction

General Introduction

The global energy sector is undergoing a profound transformation, driven by the urgent need to reduce greenhouse gas emissions, diversify energy sources, and enhance energy security. In this context, hydrogen (especially green hydrogen) has emerged as a cornerstone in the transition toward a low-carbon and sustainable energy future. As a clean and flexible energy carrier, hydrogen offers a unique opportunity to decarbonize sectors that are hard to electrify, such as heavy industry, long-distance transport, and chemical manufacturing.

Green hydrogen, produced via electrolysis powered by renewable energy, is of particular interest because it generates no carbon emissions at the point of use. Its versatility and compatibility with existing energy infrastructure make it a promising candidate for wide-scale deployment in both domestic and international energy systems.

Algeria, a country endowed with vast solar and wind resources, a robust gas and electricity network, and a strategic proximity to Europe, is well-positioned to become a major player in the global hydrogen economy. Recognizing this potential, the Algerian government launched a comprehensive National Hydrogen Strategy in 2023. This strategy envisions the development of an integrated hydrogen ecosystem capable of supplying up to 10% of Europe's hydrogen demand by 2040, while simultaneously contributing to national economic diversification, energy transition, and climate commitments [1]

However, one of the main challenges in hydrogen production via electrolysis is the availability and suitability of water resources. Given Algeria’s water scarcity, especially in the northern and southern regions, only three types of water are considered viable for large-scale hydrogen production:

- **Seawater**, primarily available in northern coastal areas.
- **Lias aquifer water**, located in the northern Sahara.
- **Albian aquifer water**, found deeper in the southern desert.

Freshwater and shallow groundwater are excluded to preserve reserves for domestic and agricultural use.

This study aims to simulate and analyze hydrogen production using Proton Exchange Membrane (PEM) electrolyzers powered by water derived from these three sources. The methodology includes a two-step simulation approach. First, water treatment processes were modeled using **DuPont's Wave** software to evaluate the performance of different membrane technologies (**Reverse Osmosis (RO)** and **Nanofiltration (NF)**) in terms of water rejection rates and specific energy consumption. Various configurations, such as one-pass and two-pass systems, were assessed to optimize energy efficiency and output quality.

Second, the simulation results namely, the water conductivity and specific energy consumption, were used as input for a dynamic model of PEM electrolyzers developed in **Simulink**. This model calculates hydrogen production rates, total energy consumption, and energy efficiency over a one-year operational period, incorporating a degradation factor to simulate membrane wear and performance loss over time.

By combining water treatment and electrolysis models, this work provides a comprehensive view of the technical and energetic feasibility of hydrogen production from alternative water resources in Algeria. The outcomes are directly aligned with the national strategy and offer practical insights for future deployment.

Chapter I

Algeria and Green Hydrogen

Chapter I: Algeria and Green Hydrogen

I.1 Algeria’s National Hydrogen Strategy

In September 2023, Algeria unveiled its National Hydrogen Strategy, a comprehensive and phased roadmap aimed at making the country a regional and global hub for the production and export of clean hydrogen. The strategy is built upon Algeria’s unique set of advantages:

- **Abundant renewable resources**: With 2,000 to 3,900 hours of sunlight per year and strong wind corridors, Algeria is well-suited for large-scale solar and wind projects.
- **Strategic geographic location**: Proximity to Europe and access to a well-developed natural gas pipeline network facilitate hydrogen export.

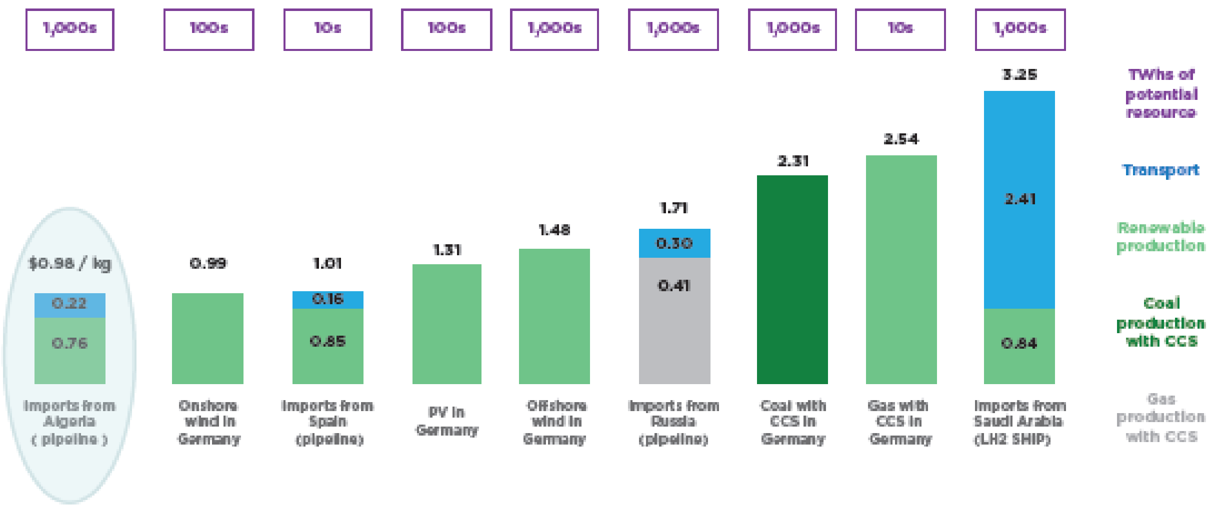

Figure I.1:Hydrogen delivery cost to Germany (Algeria: ~$0.98/kg) [1]

This figure highlights Algeria’s projected cost advantage in hydrogen delivery to Europe. The combination of cheap solar energy, proximity to European markets, and existing gas transport infrastructure allows Algeria to compete favorably against other potential exporters.

- **Industrial and scientific base**: A growing knowledge economy with more than 100 universities and active research centers in energy and environmental technologies.

Strategic Objectives

The strategy outlines the following objectives:

- Diversify Algeria's energy mix.
- Replace fossil fuels with clean hydrogen in power generation, mobility, and industry.
- Develop local value chains for electrolyzer and membrane manufacturing.
- Promote international cooperation and attract foreign investment.

A- Implementation Roadmap

The national strategy is structured into three progressive phases:

Phase 1: Demonstration and Learning (2023–2030)

- Regulatory frameworks and pilot projects (2–50 MW capacity).
- PEM electrolyzers powered by desalinated or treated aquifer water.
- Local testing of hydrogen for electricity production and mobility.

Phase 2: Industrial Deployment (2030–2040)

- Utility-scale renewable energy to power hydrogen plants.
- Production target: 40 TWh/year, with 75% allocated for export.

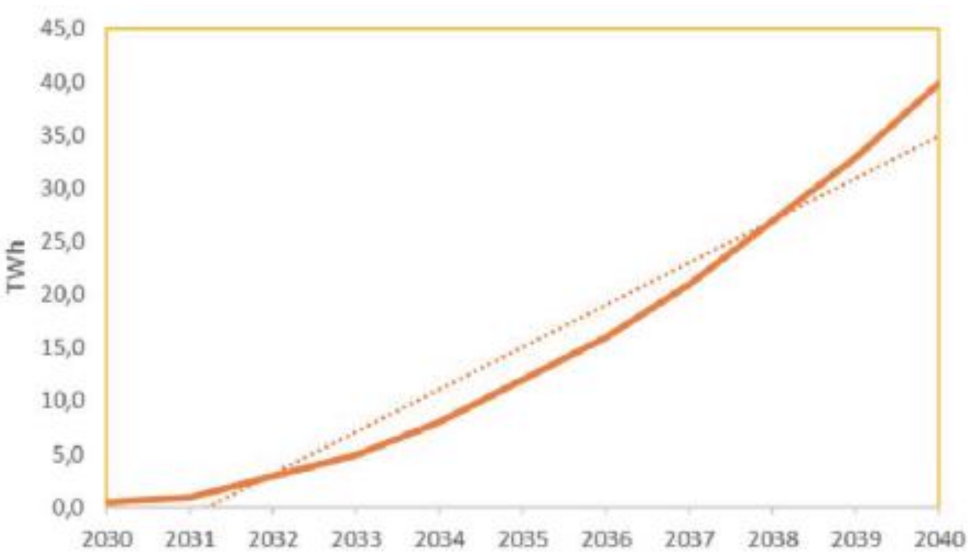

Figure I.2:Growth trajectory of hydrogen production (2023–2040) [1]

Phase 3: Export and Market Integration (2040–2050)

- Export via pipeline, ammonia, methanol, or liquefied hydrogen.
- Development of a competitive domestic hydrogen market.

B- Preferred Hydrogen Types

- **Green Hydrogen**: Electrolysis powered by solar and wind.
- **Blue Hydrogen**: Natural gas reforming with carbon capture

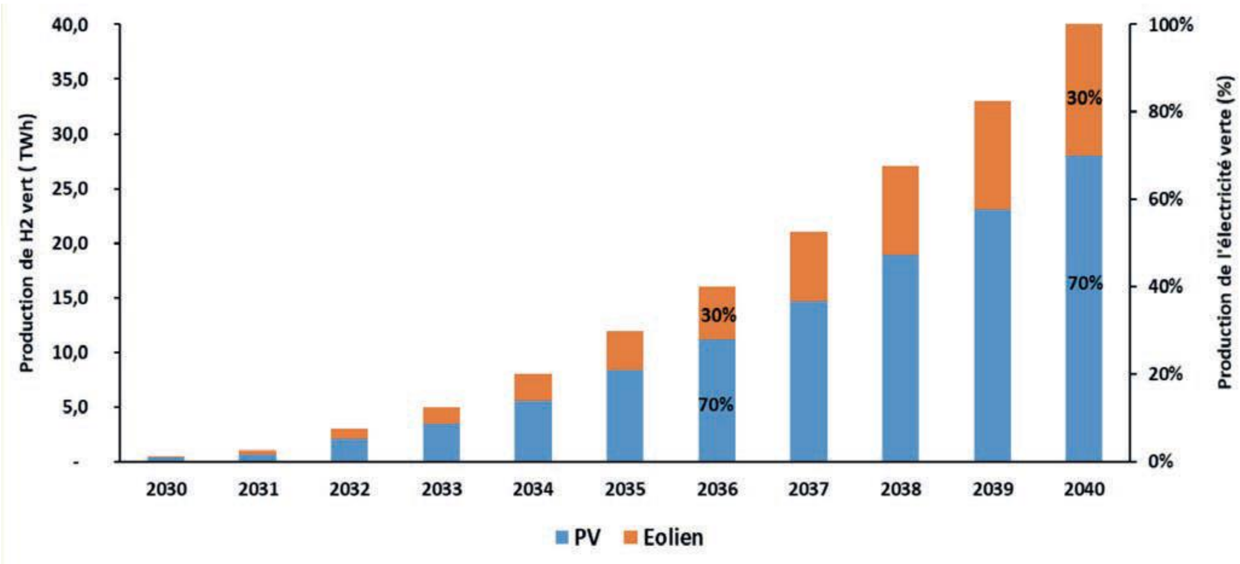

Figure I.3:Renewable electricity mix (70% solar, 30% wind) [1]

Algeria's strategy prioritizes solar power due to its high solar irradiation levels, with wind energy serving as a complementary source.

C- Water Resources and Sustainability

Given the water scarcity in Algeria, the strategy emphasizes sustainable water sourcing:

- **Desalinated seawater** in northern regions.
- **Treated wastewater** where available.
- **Deep aquifers (Lias and Albian)** in the South.

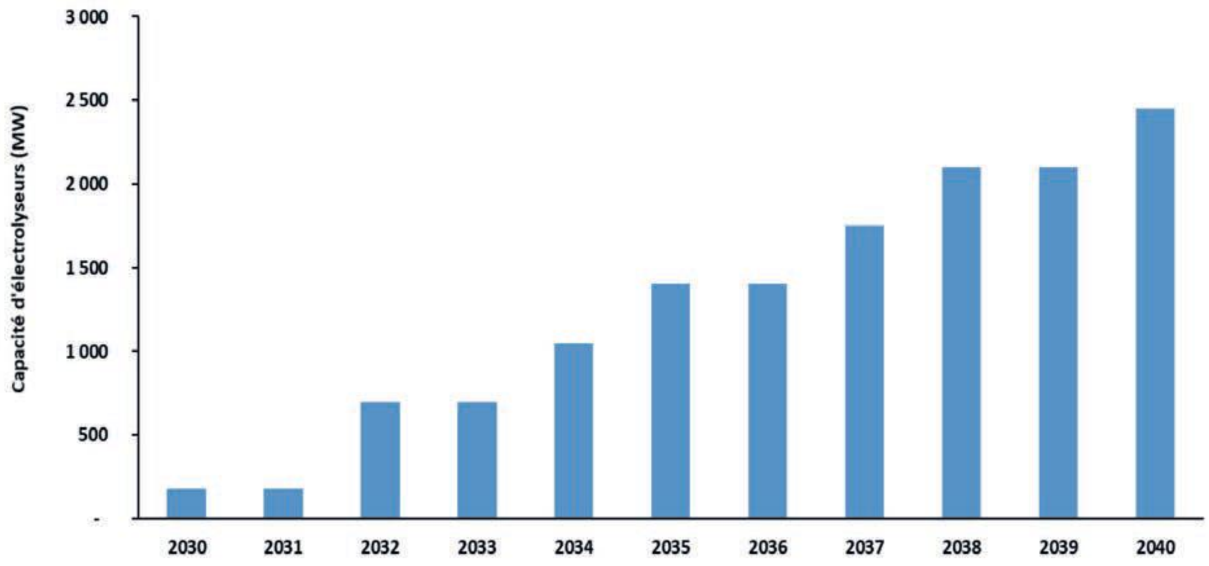

Figure I.4 Required PEM electrolyzer capacity [1]

This figure shows the installed PEM electrolyzer capacity needed to achieve the 2040 production target. It reflects the scale of investment and technology development required.

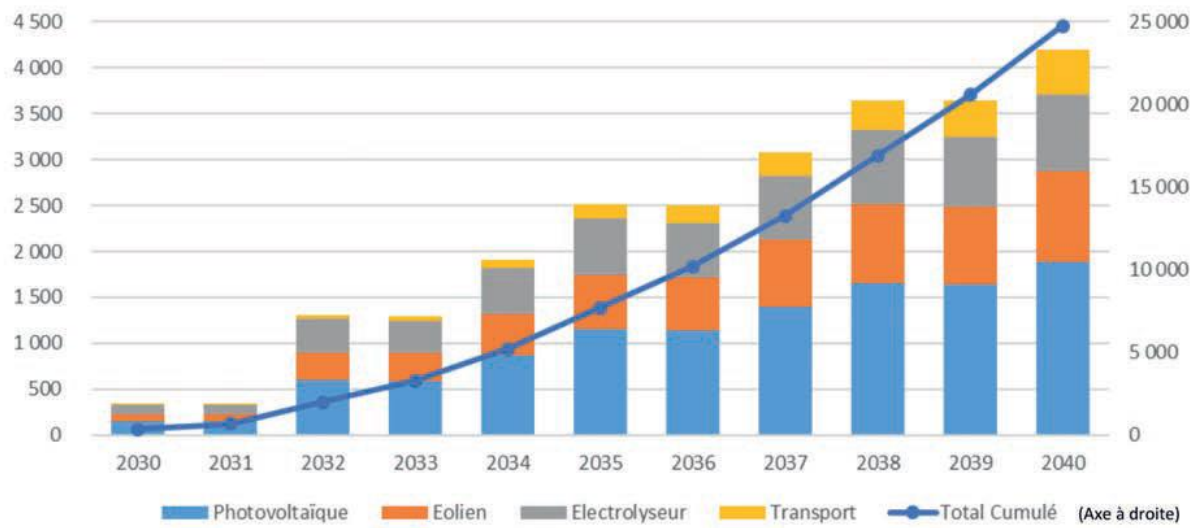

Figure I.5:Investment curve for hydrogen sector development [1]

The chart outlines Algeria's projected investment needs through 2040, estimated at $24.8 billion, excluding transport and storage.

I.2 Hydrogen presentation:

Hydrogen is a material that has been known for more than 200 years. At the beginning of the sixteenth century, Paracelsus from Switzerland discovered that gas was formed during the reaction between sulfuric acid and iron [2]. It is one of the most plentiful elements on Earth and in the Cosmos [3].

Hydrogen is an attractive alternative fuel, it can be obtained from diverse resources, both renewable (hydro, wind, wave, solar, biomass, and geothermal) and non-renewable (coal, natural gas, and nuclear) [4].

Hydrogen can also be used as a way to store energy from intermittent renewable sources, which are intermittent; the sun isn't always shining, and the wind isn't always blowing. Instead, utilities can convert the excess energy into hydrogen and then use it for energy later on, as an alternative to battery storage [5].

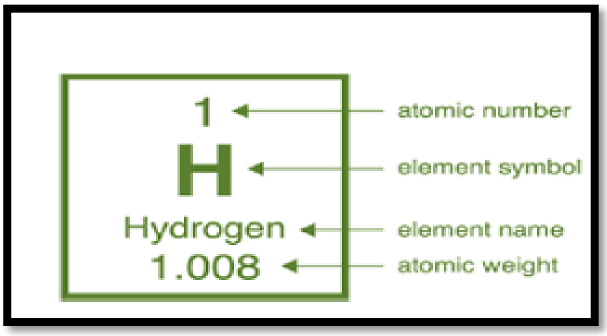

Figure I.6:Hydrogen chemical element [2]

I.3 Physical and chemical properties:

Hydrogen is the most abundant element in the universe, making up 75% of normal matter by mass, and is the third most-abundant element on the Earth's surface. Under ordinary conditions on Earth, elemental hydrogen can exist in the gas form as the diatomic molecule H2, an invisible, nontoxic, light gas. However, hydrogen gas is very rare in the Earth's atmosphere (about 1 ppm by volume) because of its light weight, which enables it to escape Earth's gravity [3].

Naturally, hydrogen exists in molecular form. It is a colorless, odorless, and tasteless gas. It changes from gas to liquid at a temperature of 252.77 °C (422.99 F) and from liquid to solid at a temperature of 259.2 °C (434.6 F). It is slightly soluble in water and alcohol. It has the lowest density (0.08999 g/L) of all elements and the ability to rapidly disperse and quickly ascend to the upper atmosphere [6].

Hydrogen is an extremely flammable gas. It burns in air and oxygen to produce water. When mixed with air and with chlorine, it can spontaneously explode by spark, heat, or sunlight. The molecular hydrogen dissociates into atomic hydrogen with a dissociation energy of around 435 kJ/mol. The atomic hydrogen is very reactive. It can bond to other atoms to make either a covalent bond or an ionic bond. In making a covalent bond, hydrogen is unusual because most atoms conform to the octet rule, ending up with eight

valence electrons; the bonding behavior of hydrogen follows the duet rule, resulting in just two electrons for bonding [6].

I.4 Type of Hydrogen:

Nowadays, most of the hydrogen produced around the world comes from fossil fuels, namely gas and coal. Depending on how it is produced in current used, hydrogen is classified into the following categories: green, yellow, pink, turquoise, brown, black, gray, red [7].

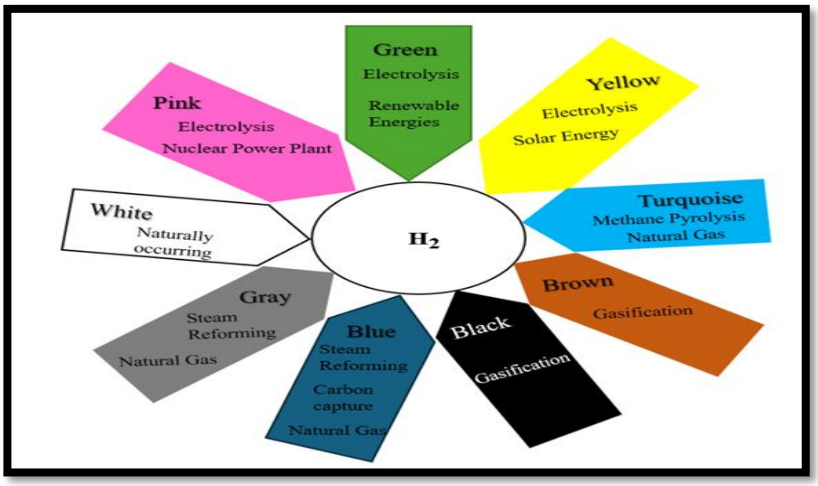

Figure I.7:The colors of Hydrogen [7]

I.4.1 Purple (Violet), Pink, and Red Hydrogen:

According to the literature, **Pink hydrogen** is generated through the electrolysis of water using electricity from a nuclear power plant. **Purple hydrogen** is made through the use of nuclear power and heat via combined chemo-thermal electrolysis splitting of water. **Red hydrogen** is produced through high-temperature catalytic splitting of water using nuclear thermal energy as the source[8].

I.4.2 Yellow Hydrogen:

Is the hydrogen that is made with electrolysis from the energy grid. The carbon emissions vary greatly depending on the sources powering the grid [9].

I.4.3 Turquoise Hydrogen:

Turquoise hydrogen is produced by the pyrolysis of methane, which can be done by thermal, catalytic, or plasma deposition [7].

I.4.4 Grey hydrogen:

Grey hydrogen is produced from fossil fuels and commonly uses the steam methane reforming (SMR) method. During this process, CO_2 is produced and eventually released into the atmosphere[8].

I.4.5 Brown and black hydrogen:

Produced from coal, the black and brown colors refer to the type of bituminous (black) and lignite (brown) coal. The gasification of coal is a method used to produce hydrogen. However, it is a very polluting process, and CO_2 and carbon monoxide are produced as by-products and released into the atmosphere [8].

I.4.6 Green hydrogen:

The State of California (2006) defined green hydrogen as being produced cleanly and sustainably, using a renewable source such as solar or wind [10]. Green hydrogen, which is also often called “clean hydrogen”, “renewable hydrogen”, or “low-carbon hydrogen”, is, by definition, the hydrogen produced with water electrolysis using electricity from renewable energy sources. By using renewable energy, green hydrogen production does not generate carbon dioxide (CO2) emissions at any point [9].

I.5 Production Methods:

I.5.1 Water electrolysis:

Water electrolysis is a process that produces hydrogen and oxygen by using electricity to split water. The main chemical reaction is as follows:

$$2H2O \ = 2H2 + \ O2 \quad [11]$$

The production of hydrogen by water electrolysis is a mature technology, based on a fundamentally simple process, is very efficient, and does not involve moving parts. It is suitable for large-scale hydrogen production. Typical efficiencies are 72%–82% [12].

I.5.2 Photocatalyst:

The term photocatalyst is a combination of two words: photo, related to photon, and catalyst, which is a substance that alters the reaction rate in its presence. Therefore, photocatalysts are materials that change the rate of a chemical reaction on exposure to light. [13]. Photolysis (or direct extraction of hydrogen from water using only sunlight as an energy source) can be accomplished by employing photobiological systems, photochemical assemblies, or photoelectrochemical cells. Intensive research activities are opening new perspectives for photoconversion, where new redox catalysts, colloidal semiconductors, immobilized enzymes, and selected microorganisms could provide means of large-scale solar energy harvesting and conversion into hydrogen.

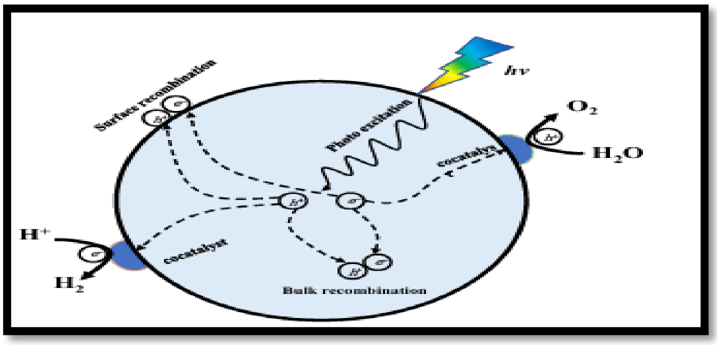

Figure I.8:Mechanism of photocatalytic water splitting for hydrogen production [14]

I.5.3 Biomass:

Using biomass as raw material can be another method used to obtain hydrogen.
Biomass gasification, involving conversion, decarbonization, and separation, is a promising approach for obtaining pure hydrogen. At the same time, hydrogen-rich compounds such as methane, methanol, or ethanol can be obtained by other processes, including enzymatic hydrolysis and fermentation. High-purity hydrogen can be reached by reforming these hydrogen compounds through catalytic reactions [9]. These different processes are summarized in Figure I.9.

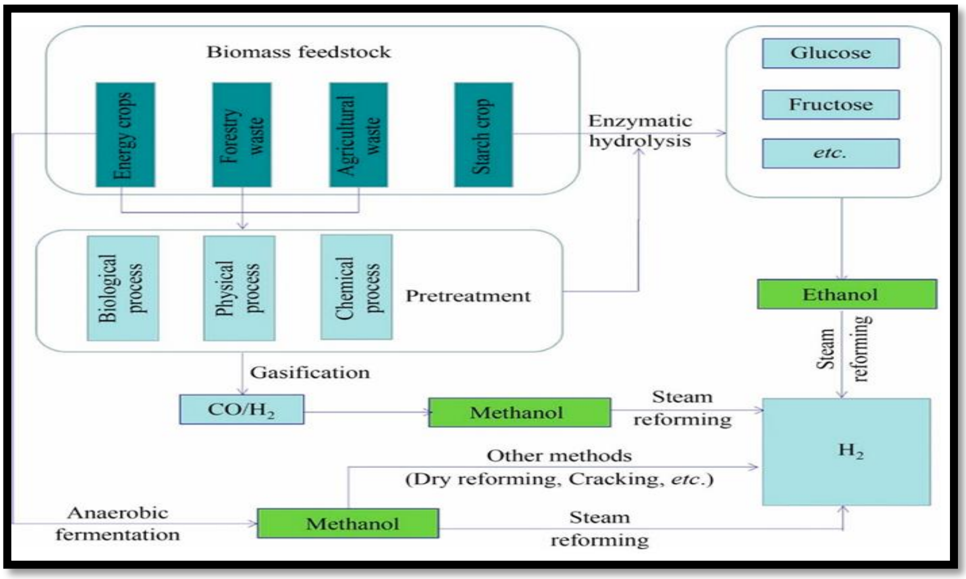

Figure I.9: Biomass Conversion Pathways for Hydrogen Production [9]

I.6 Hydrogen utilization:

Here is a brief overview of how various industries are exploring the potential of using hydrogen:

• Energy:

Green hydrogen produced from renewable sources can be stored and used to generate electricity when needed, thus ensuring a reliable and clean source of energy. Hydrogen can be used as a universal energy "preservative" since any type of energy can be converted to hydrogen energy, stored as hydrogen, and converted back into any other type of energy required. Hydrogen can be used for the conversion of low-cost electric power in excess using water electrolysis to preserve it and then convert it back to ensure additional power during peak loads, i.e., a backup power source.

• Transport:

Hydrogen fuel cell vehicles offer a zero-emission alternative to gasoline-powered cars, trucks, and airplanes. It contains three times more energy per unit mass than gasoline. Hydrogen can be used as a motor fuel in internal combustion engines (ICEs) of various vehicles with minor modifications. Hydrogen is also characterized by high combustion rate and efficiency, as well as good flammability in a mixture with air in a wide range of temperatures, thus ensuring quick engine starting at any ambient temperature.

• Industry:

Hydrogen is the most universal reagent for petroleum refining when removing sulfur compounds, nitrogen, oxygen, etc. Hydrogen is used at refineries in such processes as hydrocracking, desulfurization (hydrotreatment, hydroskimming), dearomatization, lube refining, etc. [14]

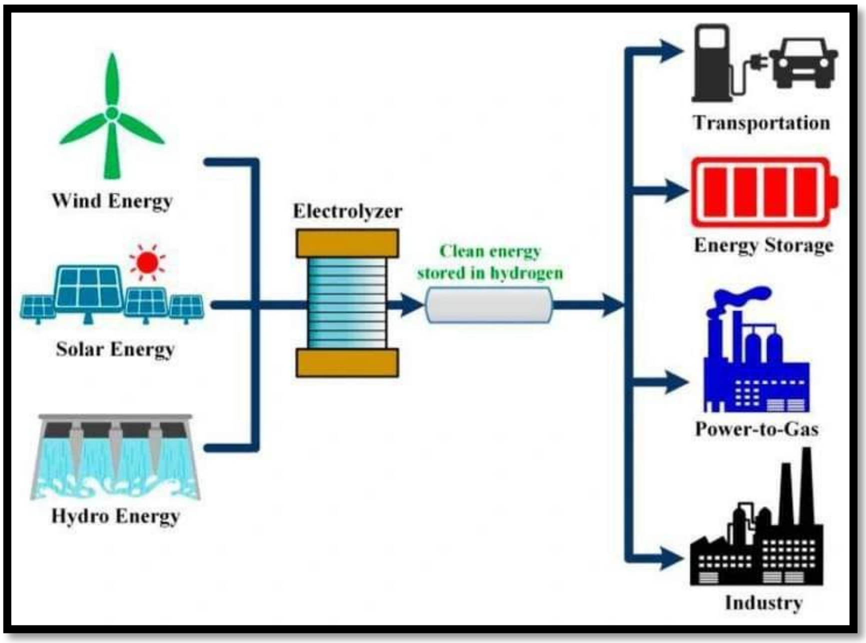

Figure I.10: Hydrogen Production from Renewables and Its Applications [15]

Conclusion:

Hydrogen is a clean and adaptable energy source with significant potential to drive the energy transition. This chapter has highlighted its essential properties, production methods, and increasing importance across different sectors. Among the various production techniques, water electrolysis emerges as one of the most promising approaches for generating green hydrogen through renewable energy sources.

Chapter II

Electrolysis

Chapter II: Electrolysis

Introduction:

Hydrogen is increasingly viewed as a key solution for replacing fossil fuels and supporting a more sustainable energy system. Among the various production pathways, green hydrogen, produced through water electrolysis using renewable electricity, stands out due to its environmental and strategic advantages. Its development requires a thorough understanding of electrochemical principles and technologies that enable efficient hydrogen production. Given the rising global interest in this sector, mastering these fundamentals is becoming essential for advancing clean energy solutions.

II.1 Principle of water electrolysis

Water electrolysis is one of the electrochemical processes. Hydrogen and oxygen are produced at the electrodes. Electrical energy is used to split water into hydrogen and oxygen according to the following reaction:

$$\mathbf{2\ H_2O + energy \rightarrow 2\ H_2 + O_2}$$

The enthalpy required for the decomposition of water at 25°C is ΔH=286 kJ/mole of H2 produced [15].

Regardless of the electrolysis method, the principal elements are always positive and negative electrodes, an electrolyte for transporting ionic currents, and a power source (DC) [16].

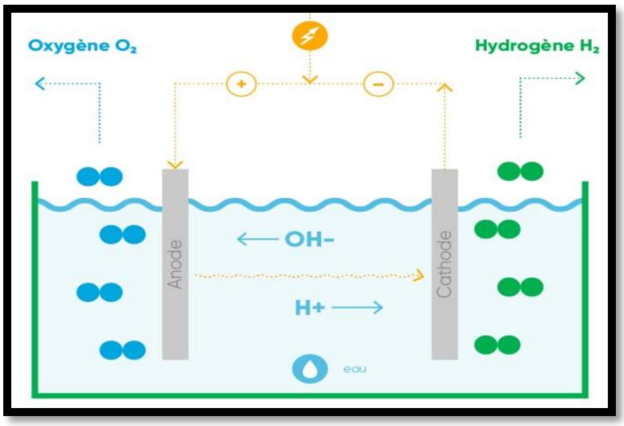

Figure II.1: Schematic Representation of the Working Principle of Water Electrolysis

II.2 Electrolysis Technologies

II.2.1 Alkaline Water Electrolysis

The AWE process, first proposed by Troostwijk and Diemann in 1789 [17], has matured alkaline electrolysis. It is now in the range of megawatts, making it the most utilized electrolytic technology at commercial levels [18].

The alkaline water electrolysis (AWE) system is usually composed of an anode and cathode immersed in an alkaline solution, generally 20%–30 % potassium hydroxide (KOH).

In this system, a diaphragm is needed to separate the two electrodes (anode and cathode). The diaphragm conducts hydroxide ions (OH-) through a KOH solution, which keeps hydrogen and oxygen separated to prevent their recombination.

The system still has some drawbacks because the diaphragm leads to high ohmic loss and limits the maximum current density. Moreover, the diaphragm cannot generate enough current to keep the hydrogen and oxygen from mixing. Therefore, a high pressure cannot be achieved, which would otherwise be beneficial for a bulky stack design.

In addition, the permeation of gas products mixes and recombines hydrogen and oxygen and decreases the Faraday efficiency [19].

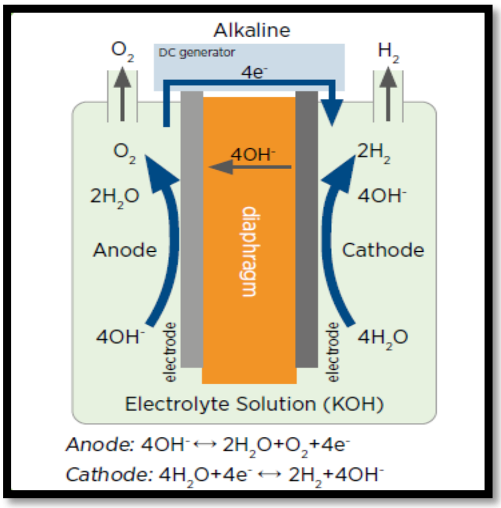

***Figure II.2: Schematic Representation of the Working Principle of an Alkaline Electrolyzer** [42]*

II.2.2 Solid oxide electrolyzers

Solid Oxide Electrolysis (SOE) is a technology employed for water steam electrolysis. It has gained significant attention for its ability to transform electrical energy into chemical energy to efficiently produce ultra-pure hydrogen.

SOE operates at high temperatures, typically in the range of 500–1000 °C, which is comparable to the output temperature of a nuclear reactor. It uses solid ceramic electrolytes, making the system compact and responsive, similar to a Polymer Electrolyte Membrane (PEM) cell.

However, SOE technology suffers from drawbacks such as electrode degradation and the use of ceramic electrolytes at temperatures exceeding 1,000 °C, which reduce their strength and stability [17].

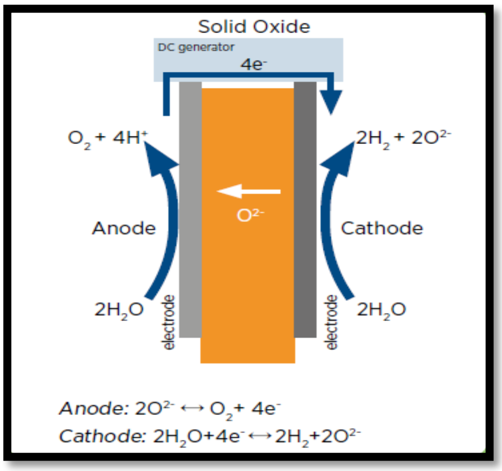

Figure II.11:Schematic Representation of the Working Principle of a Solid Oxide Electrolyzer *[42]*

II.2.3 Polymer Electrolyte Membrane Water Electrolysis

The prognosis to overcome the drawbacks of alkaline electrolysis changed when General Electric, in the 1960s, developed the first water electrolyzer based on a solid polymer electrolyte concept. This concept was idealized by Grubb, where a solid sulfonated polystyrene membrane was used as an electrolyte. This concept is also referred to as proton exchange membrane or polymer electrolyte membrane (both with the acronym PEM), water electrolysis [20]. The electrolysis reaction in the case of PEMWE proceeds with the oxidation of water at the anode, releasing O2, protons, and electrons. The protons then migrate through the solid polymer electrolyte (SPE) and reduce at the cathode, forming H2. One of the major drawbacks of PEMWE in comparison to AWE is its highly acidic nature caused by the SPE [21].

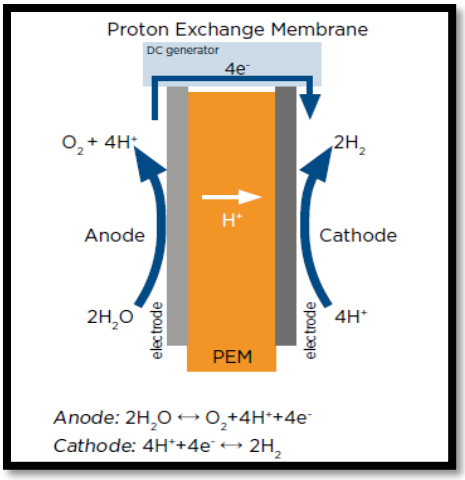

***Figure II.12:Schematic Representation of the Working Principle of a PEM Electrolyzer** [42]*

II.3. Comparison of Technologies

This table compares the key characteristics of PEM, Alkaline, and Solid Oxide electrolysis technologies. PEM offers high H_2 purity and fast start-up times, making it suitable for dynamic applications, while Alkaline systems are cost-effective with longer lifetimes. Solid Oxide electrolysis operates at high temperatures with high system efficiency but faces challenges in durability and flexibility.

Table II.1:*Characteristics of electrolysis technologies* *[20]*

	PEM electrolysis	Alkaline electrolysis	Solid oxide electrolysis
Nominal current density	1-2 A/cm²	0.2-0.8 A/cm²	0.3-1 A/cm²
Voltage range (limits)	1.4-2.5 V	1.4-3 V	1.0-1.5 V
Operating temperature	50-80°C	70-90°C	700-850°C
Cell pressure	< 30 bar	< 30 bar	1 bar
Load range	5%-120%	15%-100%	30%-125%
H2 purity	99.9%-99.9999%	99.9%-99.9998%	99.9%
Voltage efficiency (LHV)	50%-68%	50%-68%	75%-85 %
Electrical efficiency (stack)	47-66 kWh/Kg H2	47-66 kWh/Kg H2	35-50 kWh/Kg H2
Electrical efficiency (system)	50-83 kWh/Kg H2	50-78 kWh/Kg H2	40-50 kWh/Kg H2
Lifetime (stack)	50,000-80,000 hours	60,000 hours	< 20,000 hours
Stack unit size	1 MW	1 MW	5 kW
Electrode area	1,500 cm²	10,000-30,000 cm²	200 cm²
Cold start (to nominal load)	< 20 minutes	< 50 minutes	> 600 minutes
Capital costs (stack) minimum 1 MW	USD 400/kW	USD 270/kW	> USD 2,000/kW
Capital Costs (system) minimum 10 MW	700-1400 USD/kW	USD 500-1,000/kW	Unknown

Conclusion:

Alkaline water electrolysis (AWE), solid oxide electrolysis (SOEC), and proton exchange membrane (PEM) electrolysis are the primary technological pathways for green hydrogen production. Each method operates under different conditions and offers unique advantages: AWE is established and cost-effective, SOEC promises high efficiency at elevated temperatures, and PEM is noted for its compact design, high current density, and ability to respond well to intermittent renewable energy. These attributes make PEM electrolysis particularly appealing for contemporary applications that demand flexibility, efficiency, and integration with variable energy sources.

Chapter III
PEM Electrolysis for Hydrogen production

Chapter III: PEM electrolysis for hydrogen production

Introduction:

The operation of a Proton Exchange Membrane (PEM) electrolyzer is based on precise and interdependent electrochemical phenomena. Behind this promising technology lie complex anodic and cathodic reactions, advanced materials, and a delicate balance between performance and durability. Various parameters such as temperature, current density, and the quality of the feed water can significantly influence the system's behavior [22]. To better understand these interactions, several analytical and empirical models are used to represent the real behavior of the electrolyzer. A thorough exploration of these models makes it possible to evaluate how different factors affect system efficiency and degradation over time.

III.1 Structure and Functioning of a PEM Electrolyzer:

The Structure of PEM Electrolyzers consists of a stack of multiple unit cells, each having an anode and a cathode section, separated by the polymer electrolyte membrane, and sandwiched between current-distributing plates. The membrane and the electrodes are together called the Membrane Electrode Assembly (MEA). The membrane is usually made of Nafion or its derivatives, and works as a separator that keeps the anodic and cathodic products from mixing. The anode and cathode are each split into flow channels, Porous Transport Layer (PTL), and active material, as shown in Figure 3.1. The anodic flow channels are designed to ensure feed water reaches the entire active area of the electrode with uniform pressure. The cathodic flow channels, on the other hand, are designed to effectively evacuate hydrogen gas [23].

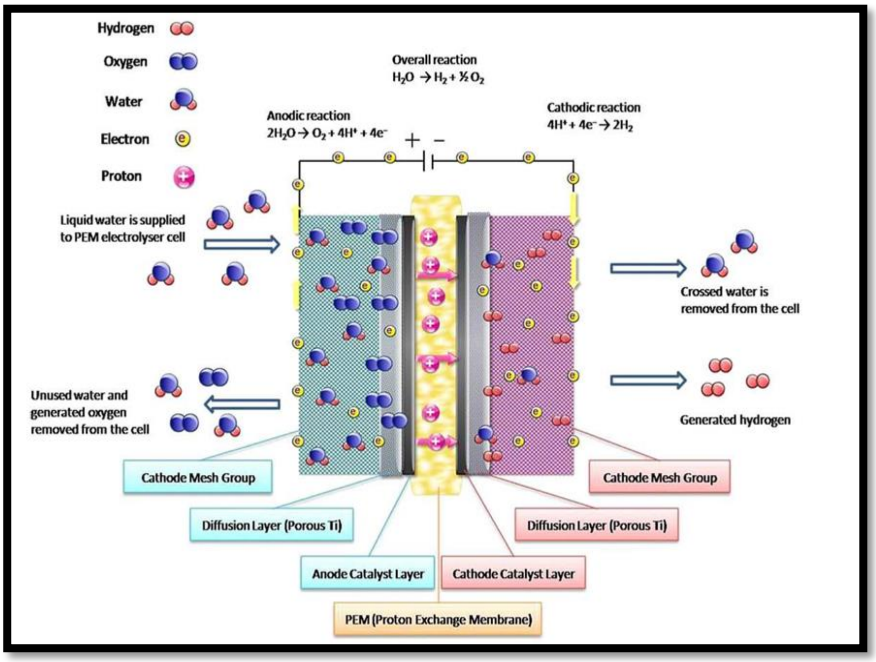

Figure III.1 Operating diagram of a PEM electrolyzer cell [52]

The protons flow through the PEM membrane, aided by the sulfonic acid groups on Nafion, while the electrons flow through the external circuit to the cathode. Hence, the membrane also works as an electrolyte. The oxygen gas is ventilated through the anodic flow channels, mixed with water vapor and traces of hydrogen that crossover through the membrane. In the cathode, the electrons from the external circuit combine with the protons from the anode and produce hydrogen gas.

III.2 Reactions:

Water is oxidized at the anode to produce oxygen, and hydrogen evolves at the cathode according to Equation [24]:

$$H_2(l) \rightarrow \frac{1}{2}O_2(g) + 2H^+ + 2e^- \quad \text{(anode)}$$

$$2H^+ + 2e^- \rightarrow H_2(g) \qquad \text{(cathode)}$$

The water fed to the anode side is split into oxygen gas, protons, and electrons. The protons are transported through the proton-conducting membrane to the cathode side. At the same time, the electrons exit the electrolyser cell via the external circuit, which supplies the driving force for the reaction, whereas at the cathode side, the protons and electrons from the external circuit recombine to form hydrogen gas [25].

III.3 Advantages and disadvantages of Proton exchange membrane electrolysis:

This table outlines the strengths and limitations of PEM electrolysis. It offers high gas purity, fast response, and compact design, making it ideal for flexible and dynamic hydrogen production. However, challenges such as high cost, limited stack size, and corrosive operating conditions may hinder large-scale deployment.

Table III.1: Advantages and disadvantages of PEM electrolysis [26]

	PEM electrolysis
Advantages	High gas purity (99.99%) Rapid system response High voltage efficiency High current densities Good partial load range Compact system design Dynamic operation Fast heat-up and cool-off time
Disadvantages	Stacks below the MW range Acidic corrosive environment Possible low durability High manufacturing cost Shorter lifetime of the stack Expensive noble metal catalysts

III.4 Parameters influencing the degradation of Proton exchange membrane electrolyzes:

The degradation of electrolysis can be linked to various factors:

III.4.1 Acidic environment and high potentials:

These conditions are inherent to PEM electrolyzers. They can lead to oxidation of PTLs and bipolar plates, as well as degrade the membrane and dissolve catalysts.

III.4.2 Temperature and pressure conditions:

Since the membrane is a polymer, high temperatures can degrade it. It is known that the membrane can withstand pressure gradients (between the anode and cathode); however, pressure cycling can have negative effects.

III.4.3 Hydration:

The membrane must remain well hydrated to ensure proper proton transport. When dehydrated, internal resistance increases, raising cell voltage and accelerating degradation mechanisms. In addition, membrane shrinkage due to a lack of water can cause cracks. This reduces its durability [27].

III.4.4 Ionic contamination:

The water circulating in the electrolyzer must be deionized. Ions dissolved in the water can contaminate the membrane or catalytic layer, increasing the cell voltage and catalyzing the production of free radicals. These ions can also come from internal components, hence the importance of choosing the right materials [28].

III.5 Models review:

Modeling a PEM water electrolyzer is essential for designing accurate and efficient control strategies. A complete model typically includes electrochemical, thermal, and H2 production sub-models [23].

III.5.1 Electrochemical models:

Electrochemical models are the heart of electrolysis modelling work to link input electrical power to output hydrogen flow [29].

The cell voltage (V_{cell}) can be expressed as the sum of several components, each representing a specific physical phenomenon or source of loss in the electrolyzer.

$$\mathrm{V_{cell}} = \mathrm{V_{rev}} + \mathrm{V_{ohm}} + \mathrm{V_{act}} + \mathrm{V_{con}} \qquad (1)$$

where,

- Reversible potential (V_{rev}) describes the required theoretical voltage, from thermodynamics, for the electrolysis reaction.

- Ohmic overpotential (V_{ohm}) models the resistance of the membrane.
- Activation overpotential(V_{act}) describes the potential needed to initiate the reaction at the electrodes.

- Concentration overpotential (V_{con})captures the voltage loss due to mass transfer limitations and the concentration gradients in the anode and cathode [30].

III.5.1.1 Reversible potential:

The Nernst equation quantifies the variation of (V_{rev}) concerning temperature and pressure:

$$V_{rev} = V_0 + \frac{RT}{2F} \ln\left(\frac{P_{H2}P_{O2}^{\frac{1}{2}}}{P_{H2O}}\right) \qquad (2)$$

Where V_0 models the reversible voltage at standard operating conditions,T is the temperature, R is the universal gas constant, and $F$is Faraday's constant. The partial pressures of hydrogen, oxygen, and water are denoted with P_{H2}, P_{O2}, and P_{H2O}, respectively [23].

Standard reversible potential is computed from the change in Gibbs free energy (ΔG), which is the energy needed to split water into gaseous oxygen and hydrogen.

$$V_0 = \frac{\Delta G}{zF} \qquad (3)$$

where (z) is the stoichiometric coefficient used to represent the number of electrons exchanged during the reaction, which is 2 for each molecule of hydrogen gas [31].

III.5.1.2 Ohmic overpotential:

Ohm's Law defines the relationship between the current and voltage of the electrolyzer with the equivalent resistance.

$$V_{ohm} = IR_{ohm} \qquad (4)$$

Where the membrane resistance,R_{ohm}, is

$$R_{ohm} = \frac{l_m}{A_m \sigma_m} \qquad (5)$$

Where $A_m(cm^2)$is the membrane section area,$l_m cm$ is the membrane thickness, and σ_m is the conductivity of the membrane, which is calculated from the water content of the membrane λ_m and the electrolyzer temperature [32].

$$\sigma_m = (0.00514.\lambda_m - 0.00326).\exp(1268.\left(\frac{1}{303} - \frac{1}{T}\right)) \quad (6)$$

III.5.1.3 Activation over potential:

The activation over potential is an energy loss in a reaction that can be described as the amount of energy required to begin the reaction [27], and is composed of $V_{act,a}$, the activation over potential for the anode, and $V_{act,c}$, the activation over potential for the cathode, such that

$$V_{act} = V_{act,a} + V_{act,c} \quad (7)$$

Based on the Butler-Volmer equation,

$$V_{act,a} = \frac{R.T}{2.\propto_a.\mathrm{F}}.\ln(\frac{i}{i_{0a}}) \quad (8)$$

$$V_{act,c} = \frac{R.T}{2.\propto_c.\mathrm{F}}.\ln(\frac{i}{i_{0c}}) \quad (9)$$

where $\propto_a$and $\propto_c$ are the charge transfer coefficients for the anode and cathode, and i_{0a} and $i_{0c}$are the respective exchange current densities [33].

For Pt-based electrodes, the current exchange densities for oxygen reduction and hydrogen oxidation reactions range between 10^{-9} _ $10^{-12}\ A/cm^2$ and 10^{-4} _ $10^{-3}\ A/cm^2$ [34], respectively. On the other hand, the values of the charge transfer coefficient for anodes and cathodes ($\propto_a$ and $\propto_c$) vary between 0 - 1 and 0-2, respectively [35]

III.5.1.4 Concentration over potential :

The concentration over potential, also denoted as the diffusion overpotential, models the resistance due to the mass transfer within the cell.

$$V_{con} = V_{con,a} + V_{con,c} \quad (10)$$

$$V_{con,a} = \frac{R.T}{z_a.F}.\ln(\frac{C_{O2,mem}}{C_{O2,mem0}}) \quad (11)$$

$$V_{con,c} = \frac{R.T}{z_c.F}.\ln(\frac{C_{H2,mem}}{C_{H2,mem0}}) \quad (12)$$

Where $C_{O2,mem}$, and $C_{H2,mem}$ are the oxygen and hydrogen concentration at the membrane-electrode interface, respectively [36].

It has been reported that V_{con} is much lower than V_{ohm}, and for this reason, many authors take $V_{con} = 0$ [23].

III.5.2 Thermal Model:

The temperature of the electrolyzer significantly affects the relationship between the voltage (V) and the current (I). To represent the behavior of the temperature and build a thermal model, it is necessary to identify all the induced heat sources [37].

$$C_t \frac{dT}{dt} = Q_{generation} + Q_{loss} + Q_{cool} \quad (13)$$

- C_t is the total thermal capacity of the electrolyzer.
- $Q_{generation}$ is the heat transfer rate generated by the chemical reaction.
- Q_{loss} is the heat transfer rate caused by the external temperature and fluid movement.
- Q_{cool} is the amount of energy required to cool down the system [37].

Where $Q_{generation}$, Q_{loss}, and Q_{cool} can be approximated from:

$$Q_{generation} = n_c(V_{cell} - V_{tn})I \quad (14)$$

$$Q_{loss} = \frac{1}{R_t}(T - T_{amb}) \quad (15)$$

Where R_t is the total thermal resistance of the electrolyzer, T_{amb} is the ambient temperature.

$$Q_{cool} = \dot{m}_c c_{c,p}(T_{c,in} - T_{c,out}) \quad (16)$$

Where, $\dot{m}_c$ and $c_{c,p}$ are the coolant mass flow rate, and specific heat, respectively, which are multiplied with the coolant temperature difference in, $T_{c,in}$, and out of the electrolyzer, $T_{c,out}$ [38].

III.5.3 Hydrogen production model:

The molar flow rates(mol/s) of consumed water and generated gases can be written following Faraday's law.

$$\dot{n}_{H2} = \frac{n_c I}{2F} \eta_F \quad (17)$$

$$\dot{n}_{O_2} = \frac{n_c I}{4F} \eta_F \quad (18)$$

$$\dot{n}_{H2O} = \frac{n_c I}{2F} \eta_F \quad (19)$$

And it can be given by [39].

$$\dot{n}_{H2} = 2\dot{n}_{O_2} = \dot{n}_{H2O} = \frac{n_c I}{2F} \quad (20)$$

Where n_c is the number of electrolytic cells associated in series and I is the current across the cell electrodes. Faraday's efficiency (η_F), defined as the relation between the real hydrogen flow rate and the theoretical one, is caused by parasitic current losses, and for PEM electrolysis, it is, in general, assumed to be more than 99% [40].

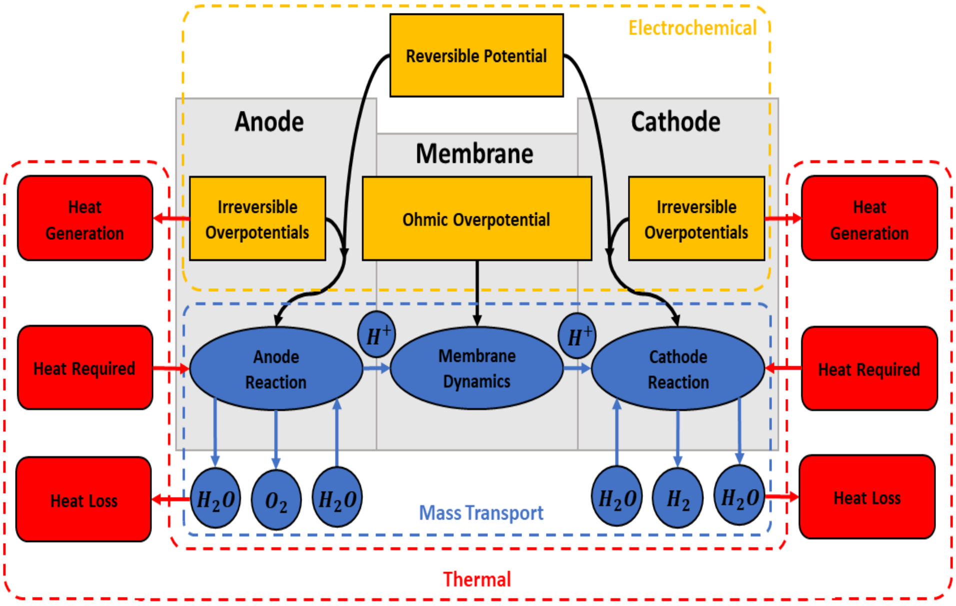

Figure III.2: Coupling of the Electrochemical, Thermal, and Mass Transport Submodels for PEM Water Electrolyzers [24].

III.6 Electrolyzer Performance:

The performance of the PEM electrolyzer was evaluated according to the energy consumption, voltaic efficiency, and electrical efficiency based on the cell voltage and amount of hydrogen produced.

The equation that was used to determine the energy consumption to produce 1 kg of hydrogen is shown below:

$$E = \frac{I_{cell} \cdot V_{cell}}{F_{H2} \cdot \rho_{H2}} \quad (21)$$

E = electrical energy consumption (kWh/kg H2)
I_{cell} = cell current (A)
V_{cell} =cell voltage (V)
F_{H2} = hydrogen flowrate (L/h)
ρ_{H2} = density of hydrogen (0.0813 kg/m3) at 1bar,25°C

The standard electrochemical potential based on the Higher Heating Value (HHV) is 1.48 V per cell. This corresponds to the thermoneutral voltage at which water is electrolyzed into hydrogen and oxygen with 100% thermal efficiency at 25 °C. At this operating point, the process does not generate excess heat. It represents the minimum theoretical voltage required for efficient liquid water electrolysis.

$$\eta = \frac{V_{TN}}{V_{cell}} \qquad (22)$$

η= cell voltaic efficiency (%)

V_{TN}=thermoneutral voltage = 1.48 V

V_{cell}=cell voltage

The energy efficiency of the PEM electrolyzer can be calculated using the following equation:

$$energy\ efficiency(\%) = \frac{HHV of H_2 production}{electrical\ energy\ cnsumption\ (kwh/kgH_2)} \times 100 \quad (23)$$

where HHV of H2 production = 39.4 kWh/kg [41].

III.7 Influence of water quality on the performance of the PEM electrolyzer:

The quality of the water used in a PEM electrolyzer has a direct impact on its efficiency and lifespan [42]. Water containing impurities or low resistivity causes an increase in cell voltage, which reduces energy efficiency and increases electricity consumption [28]. Metal ions from the water can penetrate the membrane by diffusion or under the effect of the electric field, occupying proton exchange sites and thus decreasing ionic conductivity. This leads to increased ohmic losses and accelerated membrane degradation. Poor water quality also affects the catalytic layers and porous structures (PTL), reducing overall performance [43]. Water conductivity is a key parameter to monitor: too high conductivity accelerates the degradation of internal components. To maintain good performance, the feed water must therefore have very low conductivity, in accordance with strict industrial standards [43].

Conclusion:

This chapter has identified the fundamental principles of PEM electrolysis, examining its structure, electrochemical reactions, as well as its strengths and limitations. Particular attention has been paid to degradation mechanisms and the critical influence of water quality. The introduction of modeling equations thus lays the foundation for a rigorous predictive approach. This comprehensive understanding paves the way for detailed numerical simulation of the process.

Chapter IV

Methodology

Chapter IV: Methodology

Introduction:

In order to evaluate the feasibility and performance of hydrogen production through PEM electrolysis using various water sources, a structured methodology was adopted. This approach combines water treatment simulation using DuPont's Wave software and electrolysis performance modeling via Simulink.

The selected water sources (sea water, Lias water, and Albian water) are all representative of resources available in Algeria, ensuring full relevance to the national context. For the treatment step, reverse osmosis (RO) and Nano-filtration (NF) membranes were used, tailored respectively to seawater and brackish water treatment. Various membrane configurations and rejection rates were explored to analyze their effect on treated water quality, with a special focus on conductivity.

This conductivity value is then fed into the PEM electrolysis model developed under Simulink. One of the key contributions of this model is the integration of a degradation equation that simulates the progressive performance loss of the PEM membrane over time. This degradation is modeled as a function strictly dependent on water conductivity, allowing a dynamic assessment of how feedwater quality affects long-term electrolyzer efficiency.

IV.1 Water treatment simulation:

This work involves simulating multiple water treatment scenarios using the Wave software to evaluate the suitability of different water sources available in Algeria, namely seawater, Lias groundwater, and Albian groundwater. For each source, various reverse osmosis membranes and configurations (such as single-pass and double-pass systems) are tested. The simulation outputs include the conductivity and specific energy consumption of each treatment scenario. These parameters are then used as inputs in the PEM electrolyzer model to assess their impact on system performance and energy efficiency.

IV.1.1 The software WAVE 1.82:

Description:

The WAVE software is a product launched by DUPONT Water Solutions. It is a multi-technology design software that facilitates the design of water treatment systems while optimizing performance and increasing productivity. WAVE allows for the estimation of the performance of ultrafiltration (UF), reverse osmosis (RO), and ion exchange (IX) technologies in water treatment systems, whether used individually or in combination. Additionally, the WAVE software enables a technical and economic study, along with an estimation of the cost of treated water (OPEX). Utilizing a common interface streamlines the design process and ultimately reduces the time required to manage your water treatment system. Moreover, it provides information on actual mass balance volumes and fluxes that reflect changes in density due to temperature, compressibility, and water composition.

Equations:

The performance of a specified RO system is defined by its feed pressure (or permeate flow rate, if feed pressure is not specified) and salt passage. In its simplest terms, the permeate flux Q through an RO membrane is directly proportional to the wetted area S multiplied by the net driving pressure ($\Delta P - \Delta\pi$). The proportionality constant is the membrane permeability coefficient, known as the A-value. The familiar equation for water permeation has the form:

$$\boldsymbol{Q = (A)(S)(\Delta P - \Delta\pi)} \qquad (\mathbf{24})$$

The passage of salt is by diffusion, so the flux of salt N_A is proportional to the difference in salt concentration between the two sides of the membrane. The proportionality constant is the salt diffusion coefficient, known as the B value.

$$\mathbf{N_A = \boldsymbol{B}\,(C_{FC} - C_P)} \qquad \mathbf{(25)}$$

Where:

$\boldsymbol{C_{FC}}$: average feed concentrate concentration

$\boldsymbol{C_P}$: permeate concentration

Table IV.1: Design equations for projecting reverse osmosis system performance: performance of individual elements

Object	Equation	Equation Number
Permeate flow	$Q_i = A_i \bar{\pi}_i S_E (TCF)(FF)\left(P_{fi} - \frac{\Delta P_{fci}}{2} - P_{pi} - \bar{\pi} + \pi_{pi}\right)$	26
Mean side osmotic pressure Concentrate	$\bar{\pi} = \pi_i \left(\frac{\overline{C_{fc}}}{C_f}\right)\overline{pf}$	27
Average osmotic pressure on the permeate side	$\bar{\pi} = \pi_i (1 - R_i)$	28
Ratio: arithmetic mean side Concentrate to feed the concentration for element i	$\frac{C_{fc\,i}}{C_{f\,i}} = \frac{1}{2}\left(1 + \frac{C_{ci}}{C_{fi}}\right)$	29
Ratio: concentrate to feed the concentration for element i	$\frac{C_{c\,i}}{C_{fi}} = \frac{1-Y_i(1-R_i)}{(1-Y_i)}$	30
Osmotic pressure of water Feeding	$\pi_f = 1.12(273+T)\sum m_i$	31
Temperature correction factor for RO and NF membrane	$TCF = EXP\left[2640\left(\frac{1}{298} - \frac{1}{273+T}\right)\right]; T \geq 25°C$ $TCF = EXP\left[3020\left(\frac{1}{298} - \frac{1}{273+T}\right)\right]; T \leq 25°C$	32 33
Concentration polarization factor for 8 inch elements	$pf_i = EXP[0.7Y_i]$	34
System recovery	$Y = 1 - [(1-Y_1)(1-Y_2)...(1-Y_n)] = 1 - \prod_{i-1}^{n}(1-Y_i)$	35
Permeate concentration	$C_{pj} = B(C_{fc\,j})(pf_i)(TCF)\frac{S_E}{Q_i}$	36

Table IV.2: Design equations to project system performance RO: average system performance

Object	Equation	Equation Number
Total permeate flow	$Q=N_E S_E \bar{A}\bar{\pi}(TCF)(FF)\left[P_f-\frac{\overline{\Delta P_{fc}}}{2}P_p-\pi_f\right]\left[\frac{\overline{C_{fc}}}{C_f}p_f-(1-\bar{R})\right]$	37
Ratio: average concentration between side concentrate and charge for the system	$\frac{C_{fc}}{C_f}=\frac{-\bar{R}\ln\left(1-Y/Y_L\right)}{Y-(1-Y_L)\ln\left(1-Y/Y_L\right)}+(1-\bar{R})$	38
System Recovery Limitation	$Y_L=1-\frac{\pi_f\left(\overline{pf}\right)\left(\bar{R}\right)}{pf-\Delta P_{fc}-P_p}$	39
Approximate log-mean concentration ratio concentrate side on feed for the system	$\frac{C_{fc}}{C_f}=-\frac{\ln(1-Y)}{Y}$	40
Average element recovery	$Y_i=1-(1-Y)^{1/n}$	41
Average polarization factor	$\overline{pf}=EXP\left[0.7\overline{Y_i}\right]$	42
Average concentrate-side osmotic pressure for the system	$\bar{\pi}=\pi_i\left(\frac{\overline{C_{fc}}}{C_f}\right)\overline{pf}$	43
Average concentrate-side system pressure drop for 8-inch elements; 2 steps	$\overline{\Delta P_{fc}}=0.04\bar{q}_{fc}^{\,2}$ $\Delta P_{fc}=\left[\frac{0.1\left(Q/1440\right)}{YN_{V2}}\right]\left(\frac{1}{N_{VR}}+1-Y\right)$ $\Delta P_{fc}=0.01n\bar{q}_{fc}^{\,1.7}$	44 45 46
Individual 8 inch element or single stage concentrate side pressure drop	$\bar{A}(\pi)=0.125;\pi\le 25$ $\bar{A}(\bar{\pi})=0.125-0.011\left(\frac{\bar{\pi}-25}{35}\right);25\le\bar{\pi}\le 200$ $\bar{A}(\bar{\pi})=0.070-0.0001(\bar{\pi}-200);200\le\bar{\pi}\le 400$	47 48 49

Permeability of the membrane as a function of the average osmotic pressure on the concentrate side	$C_p = BC_{fc}\overline{pf}(TCF)\left(\frac{N_E S_E}{Q}\right)$	50

IV.1.2 Characteristics of water resources:

Sea water:

This table presents the major ions in seawater, highlighting sodium (Na^+) and chloride (Cl^-) as the most abundant contributors to total dissolved solids. The high salinity, with a total of 35,962.512 mg/L, indicates the need for extensive pretreatment before electrolysis.

Table IV.3: Major Ions in sea water

Cations symbol	Composition (mg/L)	Anions symbol	Composition (mg/L)
K	408.41	CO_3	14.674552
Na	11032.981229	HCO_3	107.255217
Mg	1313.669188	Cl	19804.216
Ca	421.693826	F	1.330329
Sr	8.135474	SO_4	2775.629126
-	-	Br	68.855
Total Cations	13,184.890	Total Anions	22,771.960
Total dissolved solids	35,962.512 (mg/L)		

Lias water:

This table presents the major ions in Lias water, revealing a high total anion concentration of 2,242.631 mg/L, dominated by Cl^- and SO_4^{2-}. The elevated salinity, reflected in both anion and cation levels, indicates that advanced treatment is needed before use in electrolysis systems.

Table IV.4: Major Ions in Lias water

Cations symbol	Composition (mg/L)	Anions symbol	Composition (mg/L)
K	47.573	CO_3	0.332
Na	857.974	HCO_3	181.430
Mg	81.464	Cl	1205.993
Ca	245.386	F	87.724
Sr	4.592	SO_4	767.151
-	-	Br	-
Total Cations	1,236.990	Total Anions	2,242.631
Total dissolved solids	3,479.624 (mg/L)		

Albian water:

This table shows that Albian water has a high concentration of dissolved solids (1,580.289 mg/L), with chloride (Cl^-) and sodium (Na^+) being the dominant ions. The total anions significantly exceed the total cations, indicating ionic imbalance in raw Albian water.

Table IV.5: Major Ions in Albian water

Cations symbol	Composition (mg/L)	Anions symbol	Composition (mg/L)
K	9.588	CO_3	0.362
Na	383.537	HCO_3	274.960
Mg	43.148	Cl	625.755
Ca	95.884	F	1.043
Sr	-	SO_4	146.010
-	-	Br	-
Total Cations	532.157	Total Anions	1,048.130
Total dissolved solids	1,580.289 (mg/L)		

IV.2. Modeling the PEM electrolyser in Simulink:

In the second part of this work, the modeling and simulation of a Proton Exchange Membrane (PEM) electrolyzer were carried out using the MATLAB/Simulink environment. This simulation aims to evaluate the dynamic behavior and performance of the electrolyzer under different water quality conditions, with a particular focus on internal resistance and degradation effects.

The model is structured into several functional blocks, allowing for a modular and detailed analysis of the system. The core electrochemical behavior is represented through semi-empirical equations accounting for reversible voltage, ohmic loss, activation and concentration overpotentials. The model also incorporates mass flow calculations, power consumption, and efficiency metrics.

One of the key strengths of this modeling approach is the integration of a time-dependent degradation module. This block simulates the progressive increase in internal resistance of both the membrane and the water layer as a function of time and water conductivity. This feature makes it possible to quantify the impact of water quality on the long-term performance and durability of the PEM electrolyzer — a critical aspect when using alternative water sources such as seawater or brackish water, as available in the Algerian context.

IV.3 Presentation of the MATLAB/Simulink environment:

MATLAB Simulink Overview:

Simulink is advanced software by MathWorks Inc., which is increasingly used as a basic building block in many research areas. Simulink offers a wide perspective for the simulation and analysis of various power system networks. The features of a Simulink model are exhaustive, and at the same time, it is very easy to understand and implement. [44].

IV.4 Simulation architecture:

Block 1:

Objectif:

This block allows the initial resistances of the membrane and the water to be determined as a function of the input conductivity.

Equations:

This block uses a MATLAB Function block in Simulink to implement the semi-empirical equations of PEM electrolyzer operation.

- The cell voltage (V_{cell}):

The total relationship formula is [45]:

$$V_{cell} = V_{rev} + V_{ohm} + V_{act} + V_{con} \qquad (51)$$

Where:

$$V_{rev} = V_0 + \frac{RT}{2F}\ln\left(\frac{P_{H2}P_{O2}^{\frac{1}{2}}}{P_{H2O}}\right) \qquad (52)$$

$$\mathrm{V}_0 = 1{,}229 - 0{,}0009 \times (\mathrm{T} - 298) \qquad (53)$$

$$V_{ohm} = i\,(R_{ohm} + R_{water}) \qquad (54)$$

Current density is defined in Eq. (28):

$$i = \frac{I}{A_m} \qquad (55)$$

$$R_{ohm} = \frac{l_m}{A_m\sigma_m} \qquad (56)$$

$$R_{water} = \frac{l_{water}}{A_m\sigma_{water}} \qquad (57)$$

The conductivity of the membrane σ_m(S cm^{-1}) is [46]:

$$\sigma_m = (0.00514.\lambda_m - 0.00326).\exp\left(1268.\left(\frac{1}{303} - \frac{1}{T}\right)\right) \qquad (58)$$

An alternative model commonly used in the literature to evaluate the activation overpotential is:

$$V_{act} = \frac{R.T}{z.\propto.\mathrm{F}}.\ln\left(\frac{i}{i_0}\right) \qquad (59)$$

Where $\propto$, i_0, is the transfer coefficient and the exchange current, respectively [32].

Another model employed in the literature to compute the concentration overpotential is:

$$V_{con} = \frac{R.T}{z.\mathrm{k}.\mathrm{F}}.\ln\left(1 + \frac{i}{i_{lim}}\right) \qquad (60)$$

i_{lim} is the limiting current density based on the diffusion capabilities [47]. (with k empirical coefficient) [29]:

- Mass flow calculations [48] :

In this study, a constant current density input was applied to the PEM electrolyzer. As a result, the hydrogen production rate remained constant throughout the simulation and was calculated using Faraday's law, yielding a flow rate of approximately [$4.889 \times 10^{-3}\ Kg/h$].

$$\dot{\mathrm{m}}_{H2} = \dot{\mathrm{n}}_{H2}(\frac{\mathrm{mol}}{\mathrm{s}}) \times \mathrm{M}_{H2}(\frac{\mathrm{g}}{\mathrm{mol}}) \times (\frac{1}{1000}) \times 3600 \qquad (61)$$

$$\dot{\mathrm{m}}_{H2O\_reacted} = \dot{\mathrm{n}}_{H2O}(\frac{\mathrm{mol}}{\mathrm{s}}) \times \mathrm{M}_{H2O}(\frac{\mathrm{g}}{\mathrm{mol}}) \times (\frac{1}{1000}) \times 3600 \qquad (62)$$

$$\dot{\mathrm{m}}_{O2} = \dot{\mathrm{m}}_{H2} \times (\frac{\mathrm{M}_{O2}}{2\times\mathrm{M}_{H2}}) \qquad (63)$$

- Specific energy:

$$E_{spec} = \frac{P_{Elec}}{\dot{\mathrm{m}}_{H2}} \qquad (64)$$

With:

P_{Elec} represents the electrical power [49]:

$$P_{Elec} = V_{cell} \times I \qquad (65)$$

- Voltage efficiency:

$$\eta = \frac{V_{rev}}{V_{cell}} \qquad (66)$$

- Electrical efficiency:

$$\eta_{\mathrm{Electrical}} = \frac{\dot{\mathrm{m}}_{H2}\times HHV}{P_{Elec}} \qquad (67)$$

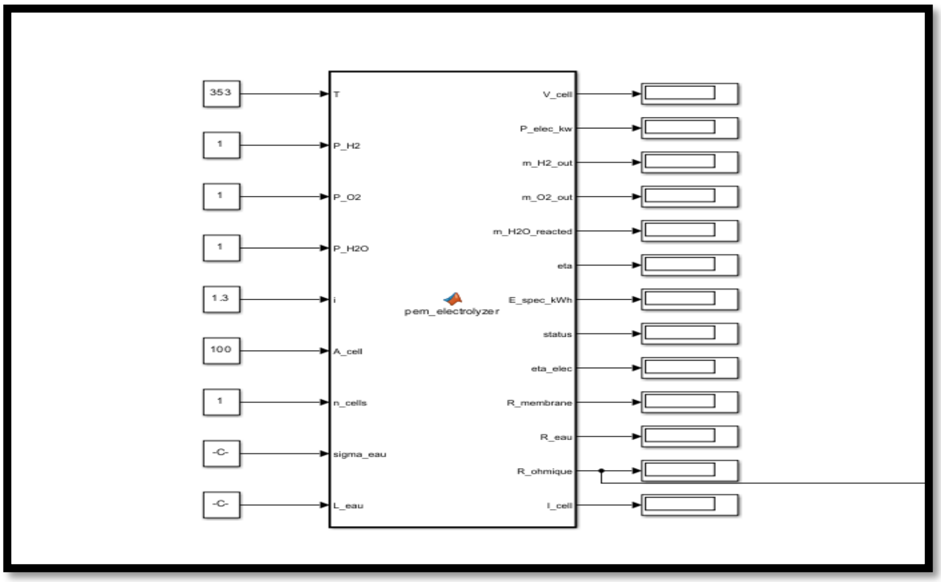

Figure IV.1: Diagram of the main modeling block of the PEM electrolyzer under Simulink

Block 2:

Objectif:

To estimate the evolution of the total internal resistance of the electrolyzer over 9000 hours of operation, the progressive degradation of both the membrane and the water layer is modeled. This time-dependent resistance is then integrated into the overall model to assess its impact on the performance of the electrolyzer.

Equations:

The equations presented below describe the time-dependent evolution of the internal resistances of the membrane and the water layer. These expressions are based on an exponential degradation model and are essential for calculating the total resistance of the electrolyzer over time.

$$R_{total} = R_{membrane} \qquad (68)$$

where R_{total} is the total resistance, $R_{membrane}$ is the resistance of the membrane.

The resistance of the membrane is calculated as follows.[50]

$$R_{membrane}(t) = R_{0_{membrane}} \times \exp(b_{membrane} \times \mathrm{t}) \qquad (69)$$

Where $R_{membrane}(t)$ is the resistance of the membrane over time, $R_{0_{membrane}}$ is the Initial Membrane resistance, and $b_{membrane}$ is the degradation rate of the .[51]

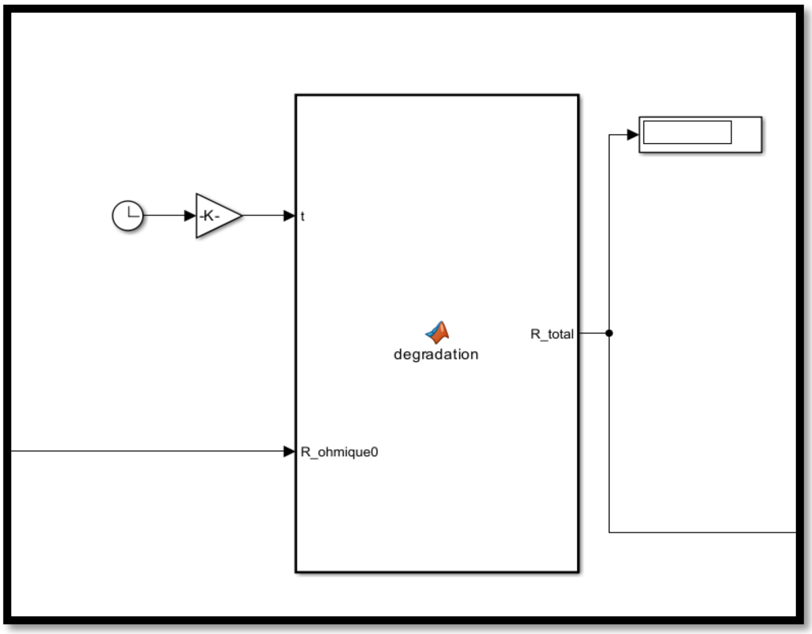

Figure IV.2: Typical block of degradation in the PEM model

Block 3:

Objectif:

To model the performance of a PEM electrolyzer by computing the cell voltage, hydrogen and oxygen production, energy use, and efficiency, taking into account operating parameters and the total internal resistance influenced by membrane and water layer.

The third block is based on the same PEM electrolyzer simulation model as the first one, but it incorporates the effects of degradation by updating the total internal resistance over time. This modification makes it possible to evaluate how membrane and water layer aging influence the electrolyzer's performance.

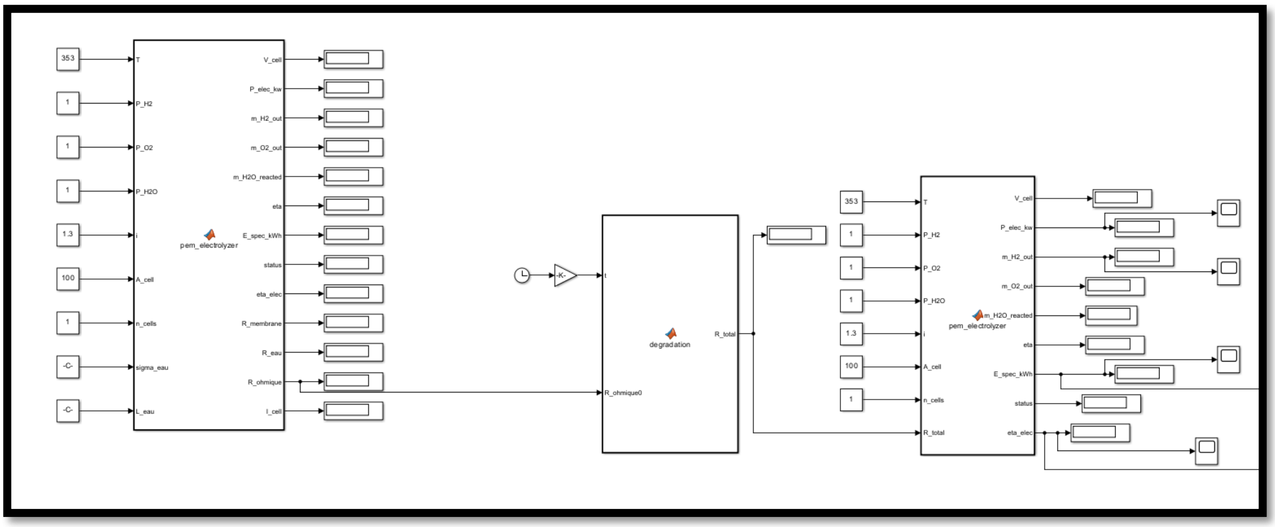

Figure IV.3: Functional Diagram of a PEM Electrolyzer with Degradation Modeling

IV.5 Input data and parameters:

Table IV.6: Input and Output Used in the PEM Electrolyzer Simulation

input	Unite SI	Output	Unite SI
Thermodynamic and Partial Parameters		Ohmic Modeling	
T: Temperature P_{H2},P_{O2},P_{H2O}: partial Pressures of Hydrogen, Oxygen, and Water Vapor	K bar	$R_{membrane}$:membrane resistance R_{water}: water resistance R_{ohm}: ohmic resistance	Ω Ω Ω
Operating and structural parameters		Mass Flow and Consumption	
i: Current density A_{cell}: cell, active area n_{cell}: Number of electrolytic cells connected in parallel.	A/cm² cm² -	Hydrogen Mass Flow Rates Oxygen Mass Flow Rates Mass flow rate of water consumed	Kg/h Kg/h Kg/h
resistor-related parameters		Performance calculation	
sigma_eau: Water Conductivity L'eau: Thickness of the water layer	S/cm cm	Cell voltage electrical power consumed Specific energy Efficiency: Voltage and Electrical Efficiency	V KW KWh/kg H_2 %

Table IV.7: Constants and values used in the PEM Electrolyzer Simulation

Constant Name	Symbol / Variable	Value	Unit	Description
Ideal gas constant	R	8.314	J/mol K	Universal gas constant
Faraday's constant	F	96485	C/mol	Electric charge per mole of electrons
Molar mass of hydrogen	M_{H2}	2.016	g/mol	Hydrogen molar mass
Molar mass of oxygen	M_{O2}	32	g/mol	Oxygen molar mass
Molar mass of water	M_{H20}	18.015	g/mol	Water molar mass
Higher heating value of H_2	HHV	39.4	kWh/kg	Hydrogen's higher heating value
Limiting current density	i_{lim}	1.401	A/cm²	Diffusion-limited current density
Empirical coefficient	k	0.315	-	For concentration overpotential
Number of electrons per reaction	z	2	-	Electrons transferred per water molecule
Charge transfer coefficient	$\propto$	0.5316	-	For activation overpotential
Exchange current density	i_0	4.576e-7	A/cm²	Exchange current density
Membrane hydration level	λ_m	22	-	Typical for Nafion membranes
Membrane thickness	l_m	0.0254	cm	Typical Nafion membrane thickness

Chapter V

Results and Discussion

V. Results and Discussions

V.1 Water treatment simulation

This section presents the simulation results of water treatment using the Wave software for three water sources: seawater, Lias water, and Albian water. The objective is to evaluate both specific energy consumption (kWh/m³) and permeate water conductivity (µS/cm) for various membrane types and system configurations (single and double pass). These results will later be used as input data for the PEM electrolyzer simulation.

For all simulations, the feed water flow rate was fixed at 10 m³/h, ensuring consistent comparison between scenarios.

Table 1 presents the key characteristics of the membranes used in the simulations. The selection includes reverse osmosis (RO) and nanofiltration (NF) membranes, categorized by their intended water type (seawater or brackish water), rejection rate, and energy specification (low, extra-low, ultra-low, or high energy). These differences strongly influence the permeate water conductivity and specific energy consumption, as discussed in the subsequent subsections.

Table V.1: Selected Membrane characteristics

Membrane series	**Type**	**Water Type**	**Rejection (%)**	**Energy Specification**
SW30HRLE-440i	RO	Sea Water	99.8	Low Energy
SW30XLE-440i	RO	Sea Water	99.8	Extra Low Energy
SW30ULE-440i	RO	Sea Water	99.7	Ultra Low Energy
SW30XHR-440i	RO	Sea Water	99.82	High Energy
Eco-Pro 440i	RO	Brackish Water	99.7	Low Energy
XLE 440i	RO	Brackish Water	99	Extra Low Energy
BW30HRLE-440i	RO	Brackish Water	99.3	Low Energy
BW30XHR-Pro 440i	RO	Brackish Water	99.7	High Energy
NF270-400	NF	Brackish Water/Sea water (Pass 2)	97	Low Energy
NF90-400	NF	Brackish Water/Sea water (Pass 2)	98.7	High Energy

V. 1.1 Case of Sea Water (TDS: 35 g/l):

Membrane effect:

This histogram illustrates (figure V.1) the effect of membrane type on specific energy consumption (in kWh/m³) and permeate water conductivity (in µS/cm) during seawater treatment with single pass and different membrane. The SW30XHR-440i (extra high rejection) membrane exhibits low conductivity (273 µS/cm) but has the highest energy consumption (4.44 kWh/m³), indicating better water quality at the expense of increased energy usage. Conversely, the SW30ULE-440i (ultra low energy) consumes the least energy (4.12 kWh/m³) but produces water with higher conductivity (611 µS/cm), reflecting a trade-off between energy efficiency and water quality in terms of low conductivity. The low-energy membranes (SW30HRLE-440i and SW30XLE-440i) demonstrate an intermediate balance.

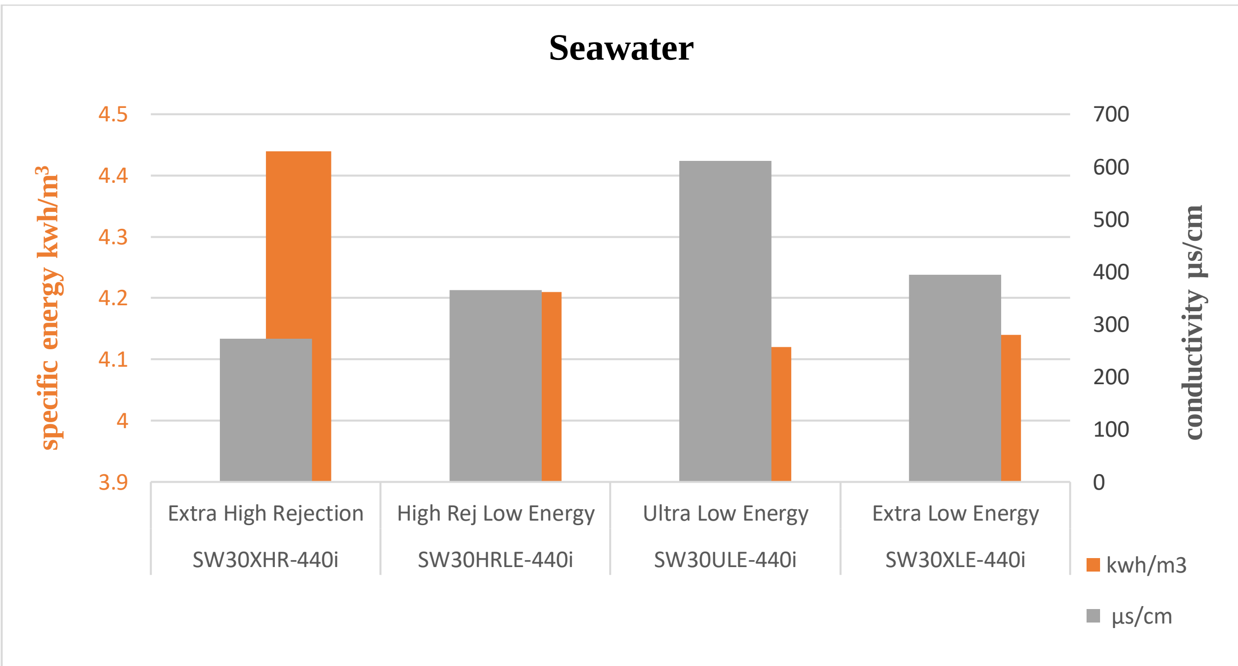

Figure V.1: Membranes effect on the specific energy and conductivity (Seawater)

Configuration effect:

The (Figure V.2) illustrates the effect of treatment unit configurations (single and double pass) on the specific energy consumption and conductivity of the permeate water during seawater treatment. The single-pass RO (XHR) system has a moderate consumption of 4.44 kWh/m³ but a relatively high conductivity of 273 µS/cm, reflecting partial ion retention. In the RO/RO bypass (XHR/XHR) configuration, the conductivity drops drastically to 2 µS/cm, indicating almost complete demineralization, but with an increased energy cost of 5.07 kWh/m³. The hybrid RO/NF system XHR/NF90 allows for a significant reduction in conductivity (35 µS/cm) while maintaining a contained energy consumption of 4.6 kWh/m³. Thus, two-pass configurations, particularly RO/NF90, provide a balanced solution between energy performance and water quality, while RO/RO is essential for applications requiring ultra-low conductivity.

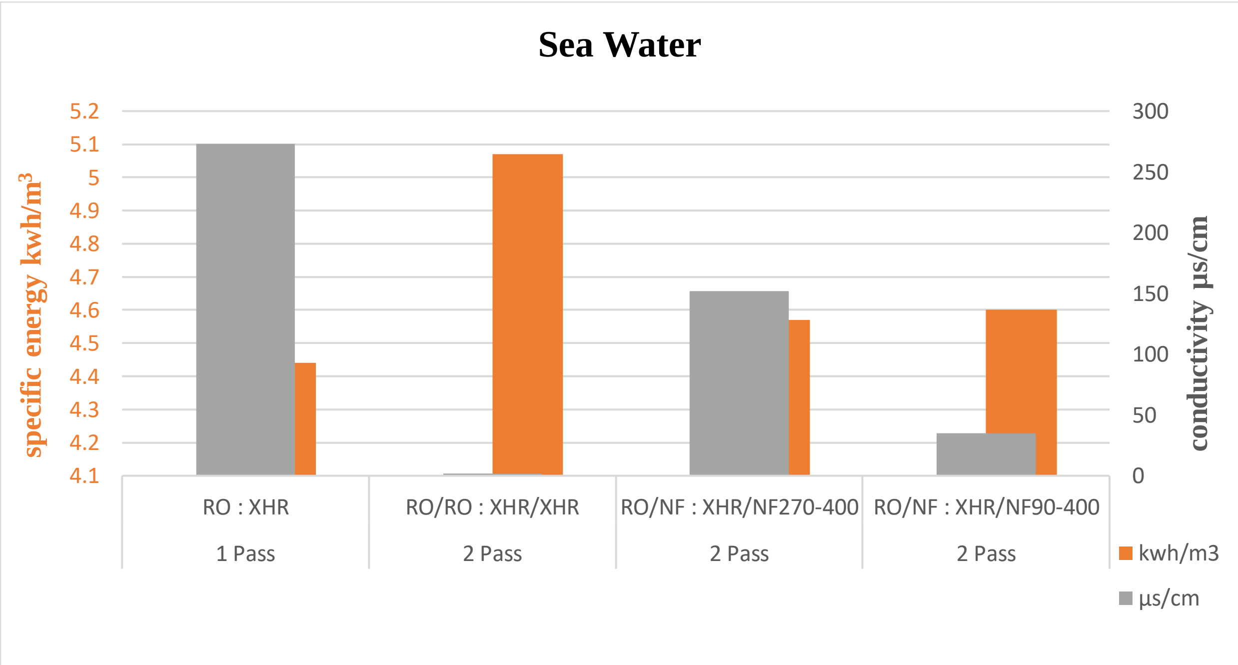

Figure V.2: Single & double pass effect on the specific energy and conductivity (SeaWater)

V. 1.2 Case of Lias Water (TDS: 3 g/l)

Membrane effect:

The (figure V.3), illustrates the effect of different membrane types on the specific energy consumption (kWh/m³) and conductivity of the treated Lias water. The XLE 440i (Extra Low Energy) membrane has the lowest energy consumption (0.51 kWh/m³), but produces water with high conductivity (274 µS/cm), indicating low salt retention. Conversely, the BW30XHR-Pro 440i (Extra High Rejection) membrane guarantees excellent water quality with minimal conductivity (51 µS/cm), at the cost of higher consumption (0.74 kWh/m³). The Eco-Pro 440i and BW30HRLE-440i membranes offer a good compromise with moderate consumption (0.62 kWh/m³) and acceptable conductivity levels (107 and 136 µS/cm, respectively). Therefore, the choice of membrane depends on the requirements for water quality and energy efficiency. For low-mineralized water, the BW30XHR-Pro membrane remains the most efficient despite a higher energy cost.

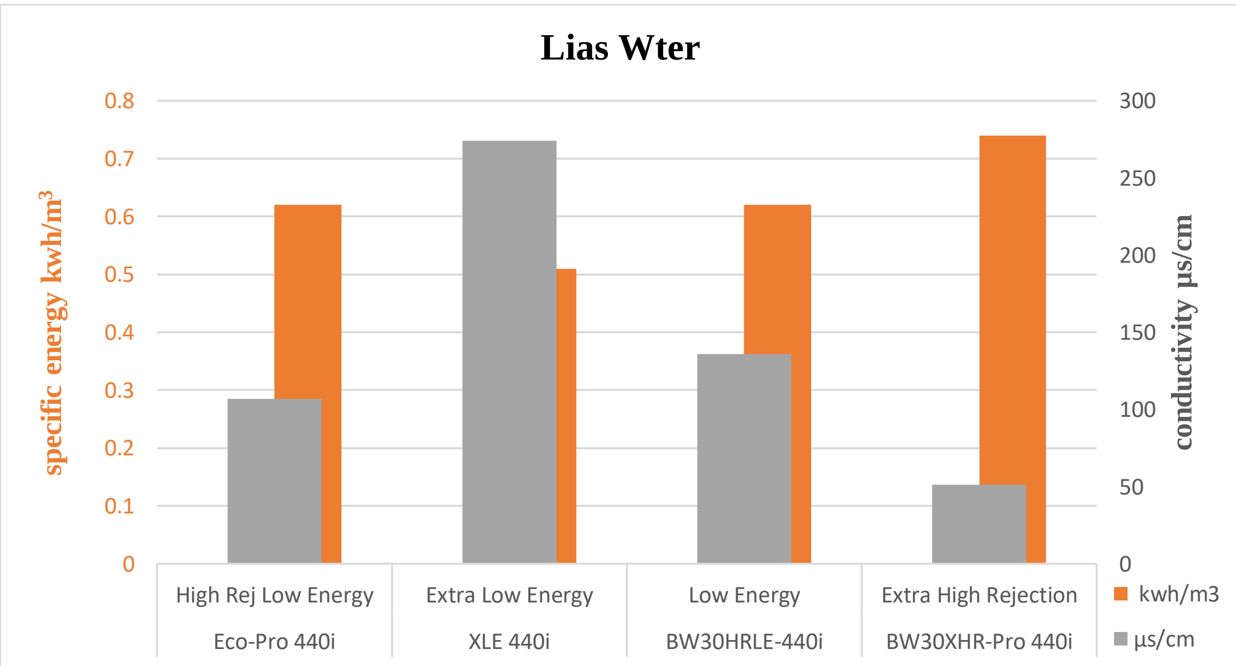

Figure V.3: Membranes effect on the specific energy and conductivity (LiasWater)

Configuration effect:

The (figure V.4) is displaying the effects of various reverse osmosis (RO) and nanofiltration (NF) treatment configurations on Lias water regarding specific energy consumption (kWh/m³) and final water conductivity (µS/cm). The 1-pass RO: XHR system has moderate energy consumption (0.74 kWh/m³) but high conductivity (51 µS/cm), indicating partial treatment. In comparison, the two-pass RO/RO: XHR/XHR configuration achieves the lowest conductivity (5 µS/cm), but at the cost of high specific energy (1.08 kWh/m³), which indicates excellent water quality but low energy efficiency. The hybrid RO/NF configurations: XHR/NF90-400 offer an interesting compromise by reducing energy consumption (0.89 kWh/m³) while ensuring relatively low conductivity (9 µS/cm). Among these options, the XHR/NF90-400 configuration appears optimal for balancing water quality and energy performance.

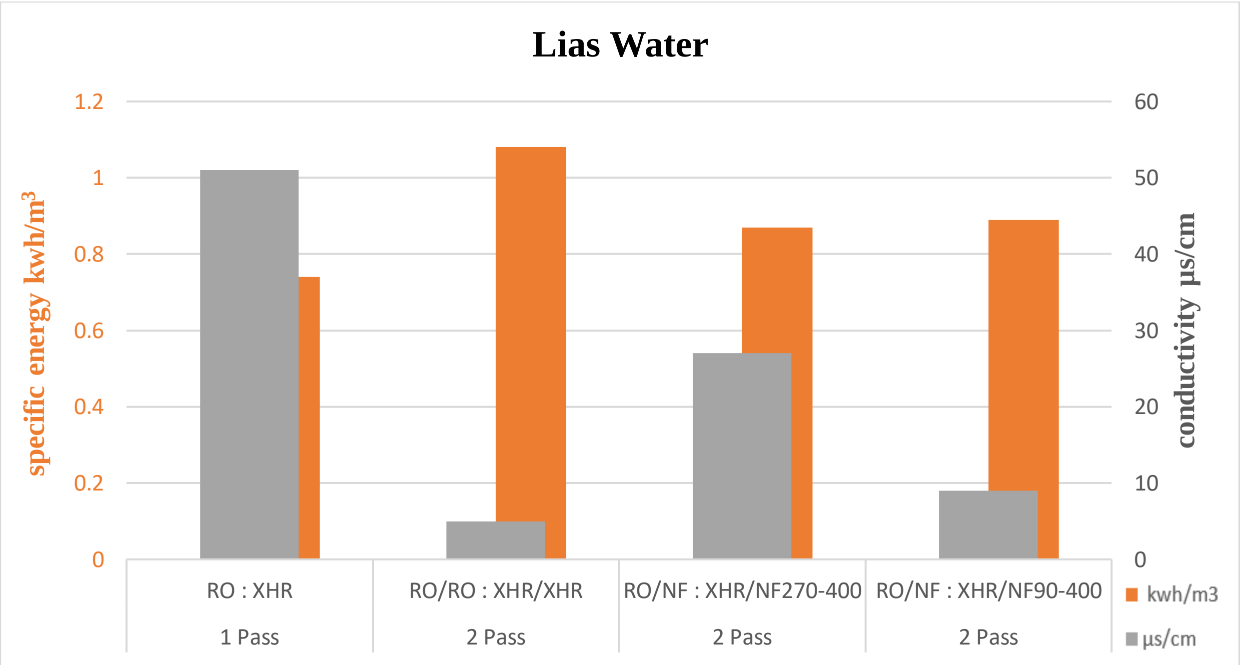

Figure V.4: Single & double pass effect on the specific energy and conductivity(LiasWater)

V. 1.3 Case of Albian Water (TDS: 1.5 g/l)

Membrane effect:

This chart (figure V.5) compares four membrane types based on specific energy consumption (kWh/m³) and conductivity (µS/cm). The XLE 440i has the highest conductivity despite low energy use, indicating poor rejection. In contrast, BW30XHR-Pro 440i shows excellent water purity (lowest conductivity) but at the highest energy cost. Eco-Pro 440i and BW30HRLE-440i offer balanced performance with moderate energy and conductivity values. Overall, membranes with higher rejection tend to require more energy.

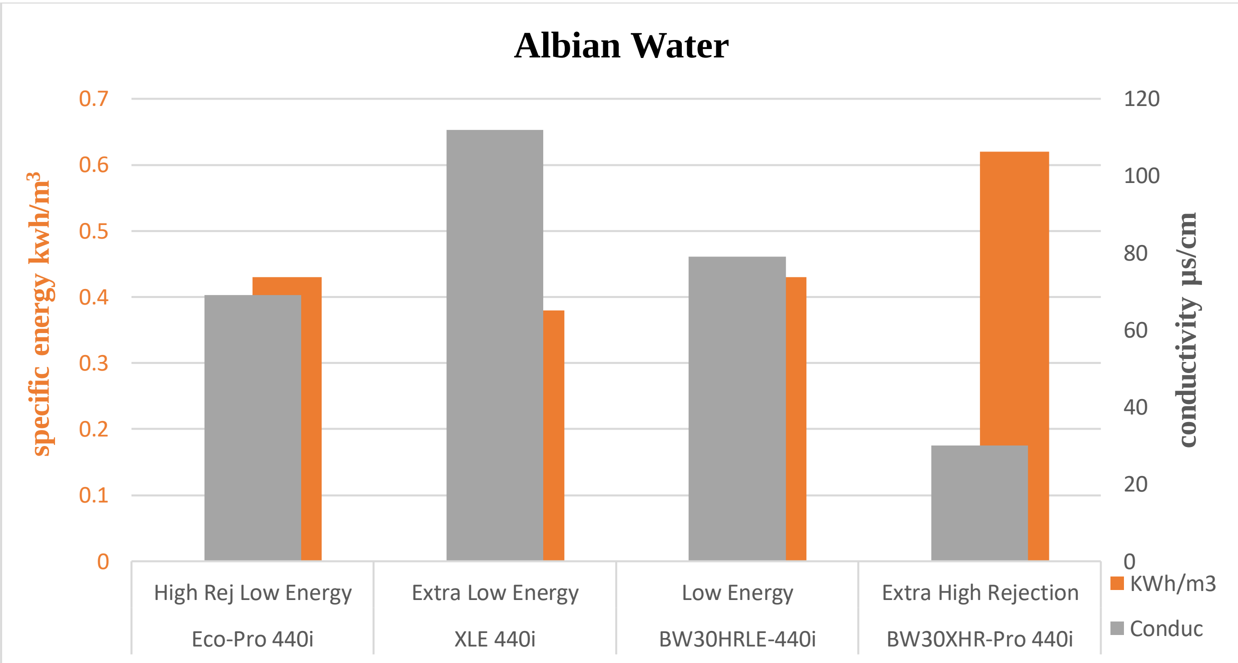

Figure V.5: Membranes effect on the specific energy and conductivity(AlbianWater)

Configuration effect:

The (figures V.6), compares specific energy consumption (kWh/m³) and conductivity (µS/cm) across different water treatment configurations. The RO: XHR (1 Pass) setup shows the highest conductivity and energy usage. Introducing a second pass with combined RO or NF stages significantly reduces conductivity, indicating better water purity. The RO/NF: XHR/NF90-400 system achieves the lowest conductivity and energy demand, making it the most efficient. Overall, multi-pass hybrid systems offer better performance with lower energy use and higher water quality.

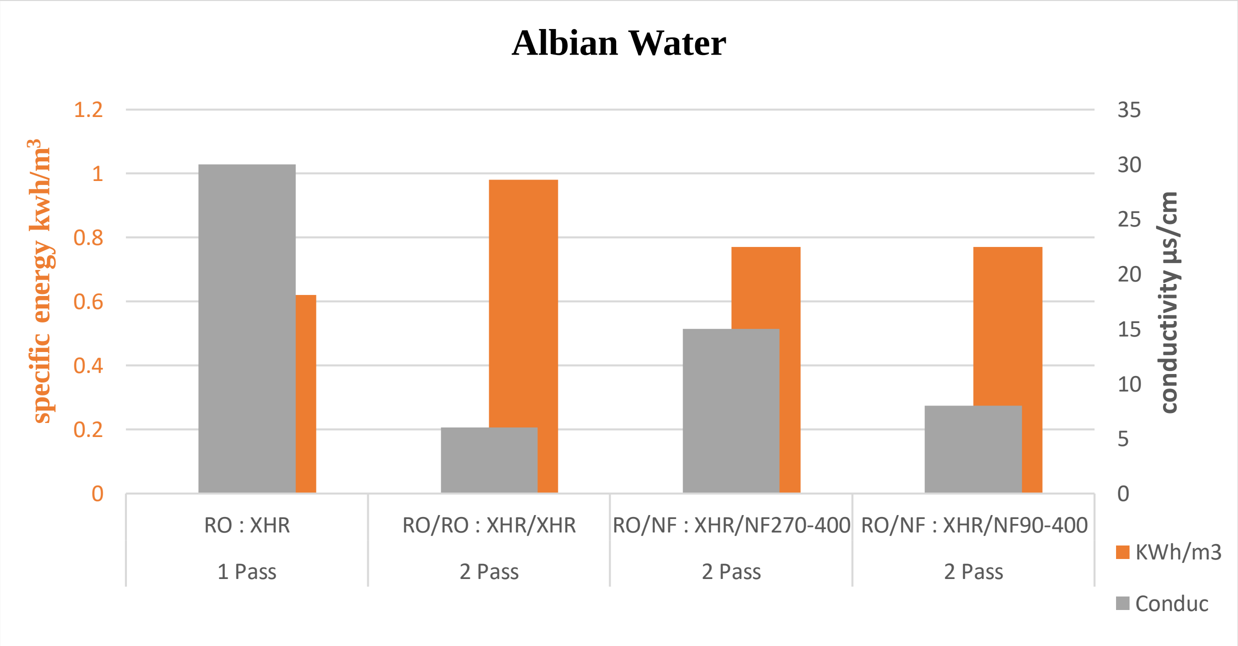

Figure V.6: Single & double pass effect on the specific energy and conductivity(AlbianWater)

V. 2 Comparative Conclusion on Water Treatment Simulation

The simulation results reveal that membrane selection and system configuration play a pivotal role in optimizing both specific energy consumption and permeate water quality across the three water sources studied: seawater, Lias, and Albian.

For seawater (TDS = 35 g/L), the SW30XHR-440i membrane in a double-pass hybrid configuration (RO/NF90) was the most efficient compromise, significantly reducing conductivity from 273 µS/cm to 35 µS/cm while maintaining a reasonable energy consumption of 4.6 kWh/m³.

The RO/RO configuration, while providing ultra-low conductivity (2 µS/cm), imposed a higher energy burden (5.07 kWh/m³), making it suitable only for applications requiring ultrapure water.

In the case of Lias water (TDS = 3 g/L), the BW30XHR-Pro 440i membrane in combination with an XHR/NF90-400 system achieved excellent water quality (9 µS/cm) at a relatively low energy cost (0.89 kWh/m³), outperforming single-pass setups in both aspects. This configuration offers a balanced solution for treating moderately saline water where both energy efficiency and low mineral content are desired.

For Albian water (TDS = 1.5 g/L), similar trends were observed. The RO/NF90 hybrid system again outperformed others, yielding high-quality water with minimal conductivity and the lowest specific energy consumption among all double-pass configurations. Simpler systems, such as RO: XLE, were more energy-efficient but insufficient in terms of salt rejection.

Overall, double-pass hybrid configurations (RO/NF90) proved to be the most suitable for all water types studied, offering an optimal trade-off between energy efficiency and water purity. These results validate the selection of the XHR/NF90-400 configuration for the next phase of the study, which involves PEM electrolyzer simulation, ensuring that the input water quality is sufficiently high for efficient hydrogen production.

V. 3 PEM Electrolyzer simulation

This section presents the simulation results of a PEM electrolyzer fed with permeates derived from different water sources (seawater, Lias water, and Albian water). For each case study, we analyze the energy performance based on the type of membrane used and the water treatment configuration (single pass, double pass, nanofiltration, etc.). The objective is to evaluate how the feed water conductivity influences the specific energy consumption (kWh/kg H_2) and the electrolyzer's efficiency over time.

The results highlight the relationship between the treated water quality (particularly its conductivity) and the operational performance of the electrolyzer. While several configurations were tested for each water source, only the most optimal systems (i.e., those offering the best compromise between energy consumption and long-term stability) were selected for the final comparison. These insights are essential to guide technological choices depending on the available water resource, especially in the context of optimizing green hydrogen production.

V. 3.1 Case of seawater permeate

Figure V.7 illustrates the evolution of specific energy consumption (kWh/kg H_2) over time, influenced by the conductivity of water produced by different membranes. The permeate from the SW30ULE-440i membrane (611 µS/cm) enables low energy demand during the initial 450 hours. However, after this period, the energy requirement rises sharply. This behavior can be attributed to the increased degradation rate of the PEM electrolyzer components when exposed to higher ion concentrations. Conversely, the SW30XHR membrane (273 µS/cm), which delivers lower conductivity water, initially requires slightly more energy but ensures much greater operational stability over the long term, particularly beyond 500 hours, by reducing membrane and electrode deterioration.

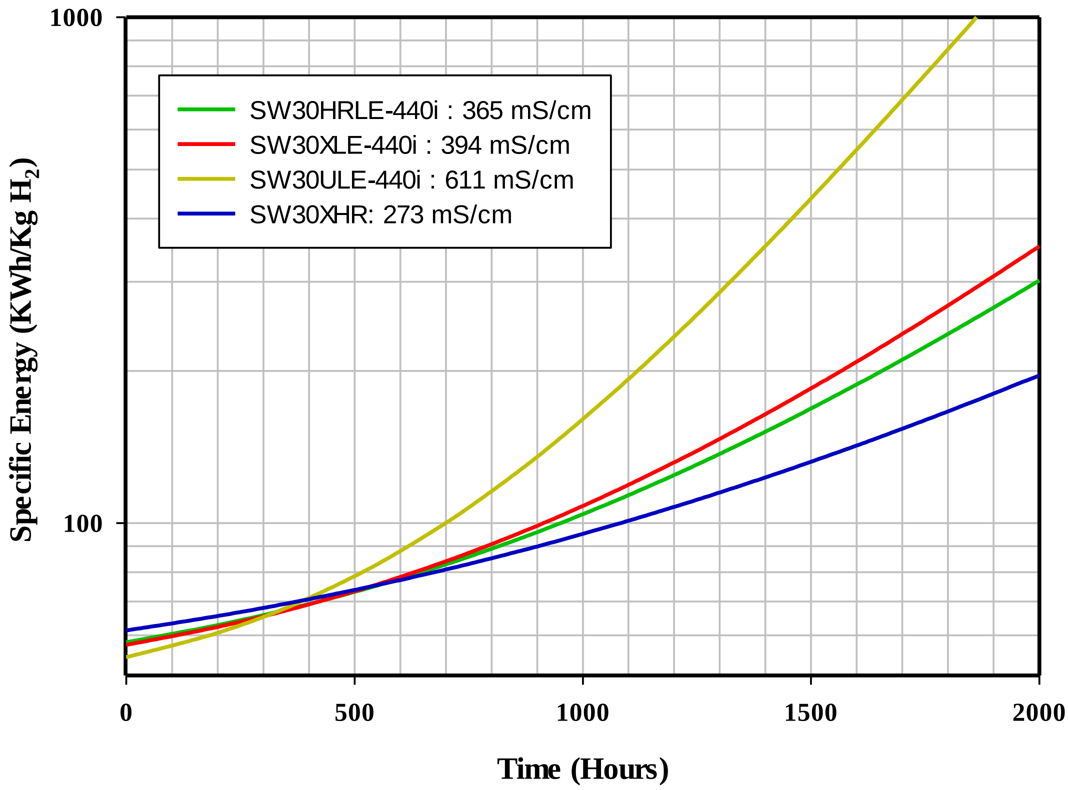

Figure V.7: Specific energy vs. time: Membrane type effect for seawater permeate

Figure V.8 presents the impact of different water treatment configurations on specific energy consumption over time. The single-pass XHR system using a high-rejection membrane (273 µS/cm) experiences a marked increase in energy demand after 4000 hours, indicating early degradation. The double-pass XHR/XHR system (2 µS/cm) maintains better stability but at the cost of significantly higher energy consumption due to the extremely low conductivity. The double-pass XHR/NF270 configuration with 152 µS/cm shows moderate degradation, while the same configuration delivering a conductivity of 35 µS/cm achieves the best compromise, offering reduced energy usage and improved long-term consistency, thanks to an optimal conductivity level that supports efficient electrolysis without accelerating system fatigue.

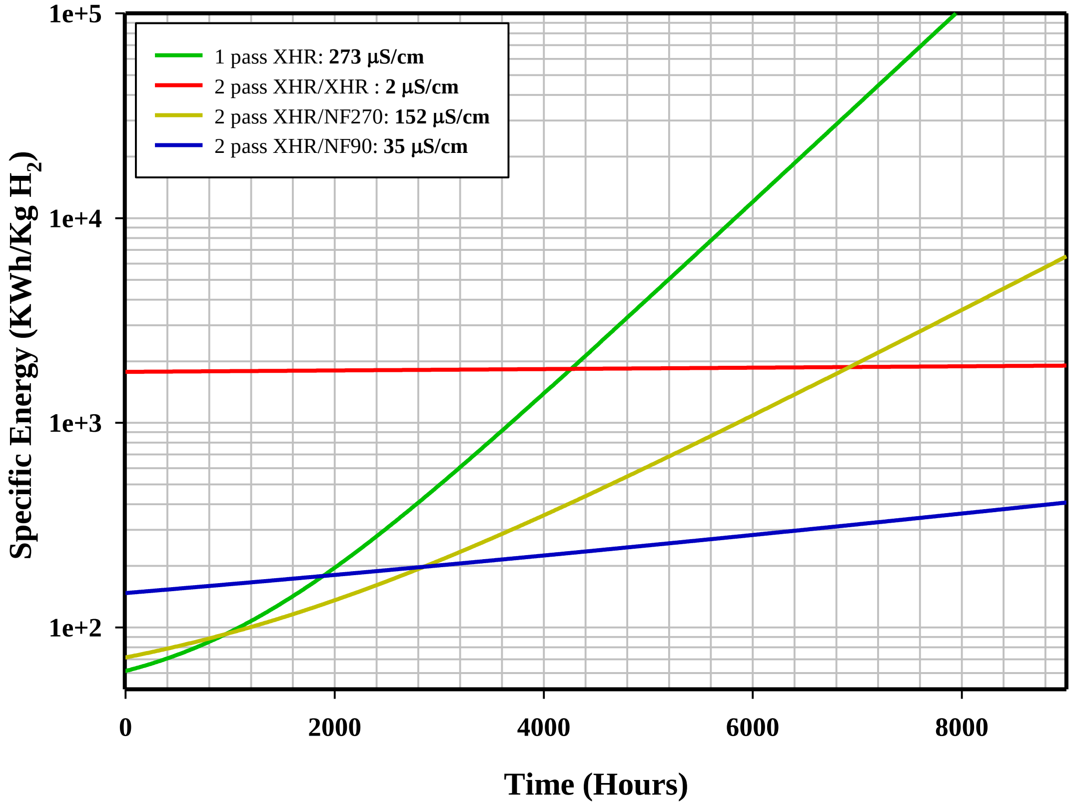

Figure V.8: Specific energy vs. time: configuration effect for Seawater permeate

Figure V.9 further explores the energy efficiency of the PEM electrolyzer under various water conductivities. As expected, the XHR/XHR configuration (2 µS/cm) leads to the lowest and most stable efficiency due to excessive water purity, which limits ion transport and increases ohmic resistance. In contrast, the XHR/NF90 configuration at 35 µS/cm maintains high and stable efficiency over time, illustrating an ideal balance between conductivity and electrochemical compatibility. The single-pass XHR (273 µS/cm) and XHR/NF270 (152 µS/cm) systems exhibit a rapid drop in efficiency after 2000 hours, showing their limited suitability for long-term hydrogen production from seawater.

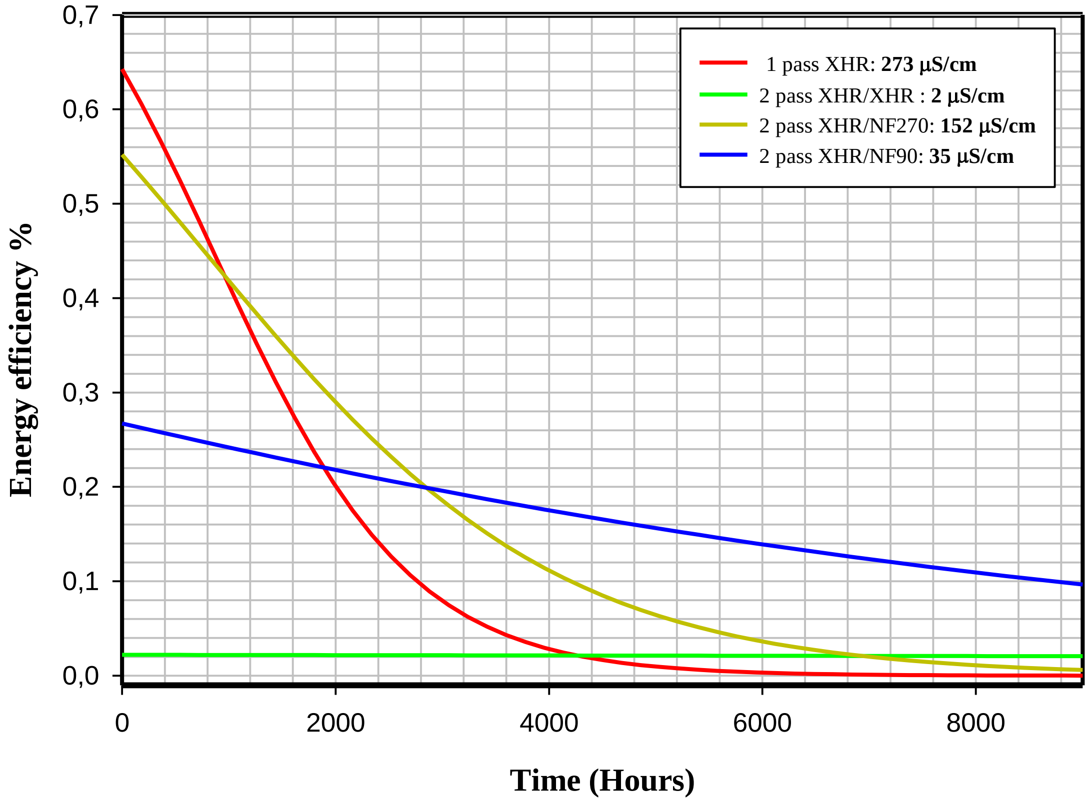

Figure V.9: Energy efficiency vs. Time for different membranes and unit configuration: Seawater

V. 3.2 Case of Lias water permeate

Figure V.10 illustrates how specific energy consumption evolves over time depending on the membrane used to treat Lias water. Initially, the BW30XHR-Pro 440i membrane (51 µS/cm) exhibits the highest energy consumption due to its very low conductivity. However, this configuration demonstrates excellent long-term stability and surpasses the others after 3000 hours. In contrast, the XLE 440i membrane (274 µS/cm) shows rapid degradation with a steep increase in energy demand after only 2000 hours, highlighting its limited durability. The BW30HRLE-440i (136 µS/cm) and Eco-Pro 440i (107 µS/cm) offer intermediate performance: lower initial energy demand but with gradual degradation over time. These observations emphasize the importance of finding a balance between conductivity and membrane endurance.

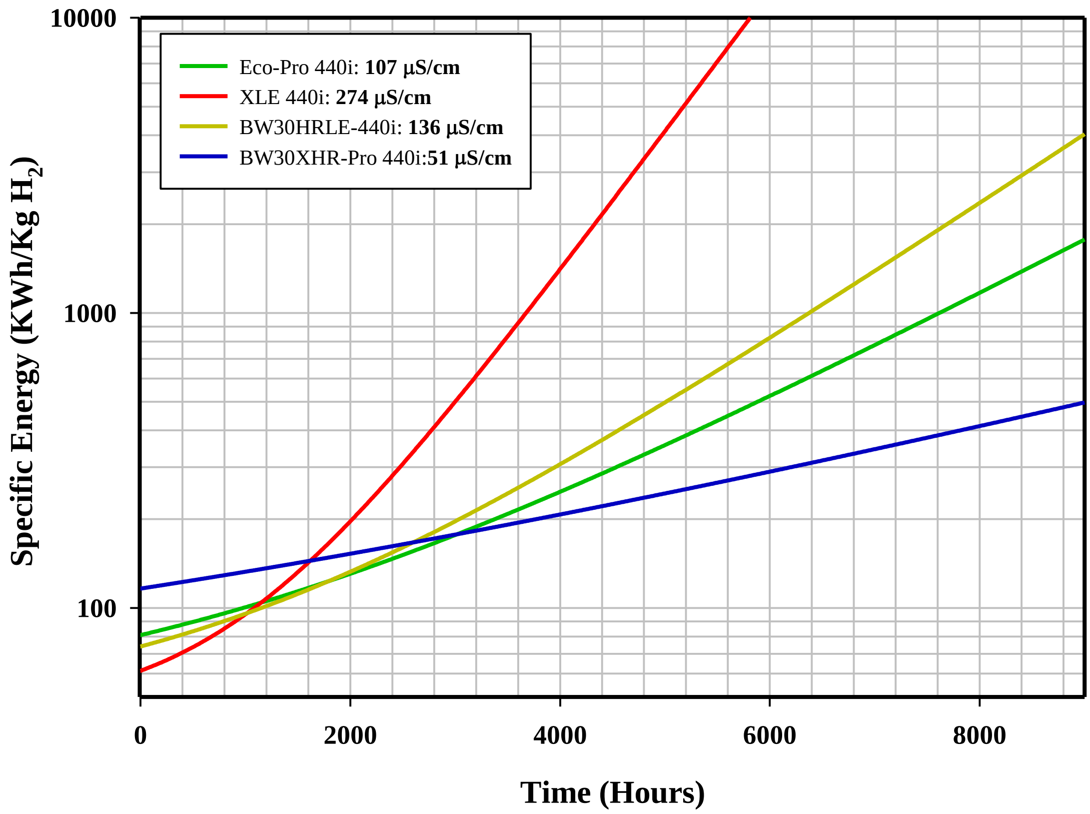

Figure V.10: Specific energy vs. time: Membrane type effect for Lias water permeate

Figure V.11 analyzes various treatment configurations and their impact on specific energy consumption. The single-pass XHR system initially appears most energy-efficient but shows a steep rise in consumption, reflecting rapid system fatigue. The double-pass XHR/XHR configuration achieves the highest water purity but also requires significantly more energy. On the other hand, the double-pass XHR/NF270 systems deliver moderate and more stable performance. In particular, the configuration producing a permeate at 9 µS/cm achieves the best overall result, combining low energy use with long-term operational stability, thus representing the most favorable option for hydrogen production from Lias water.

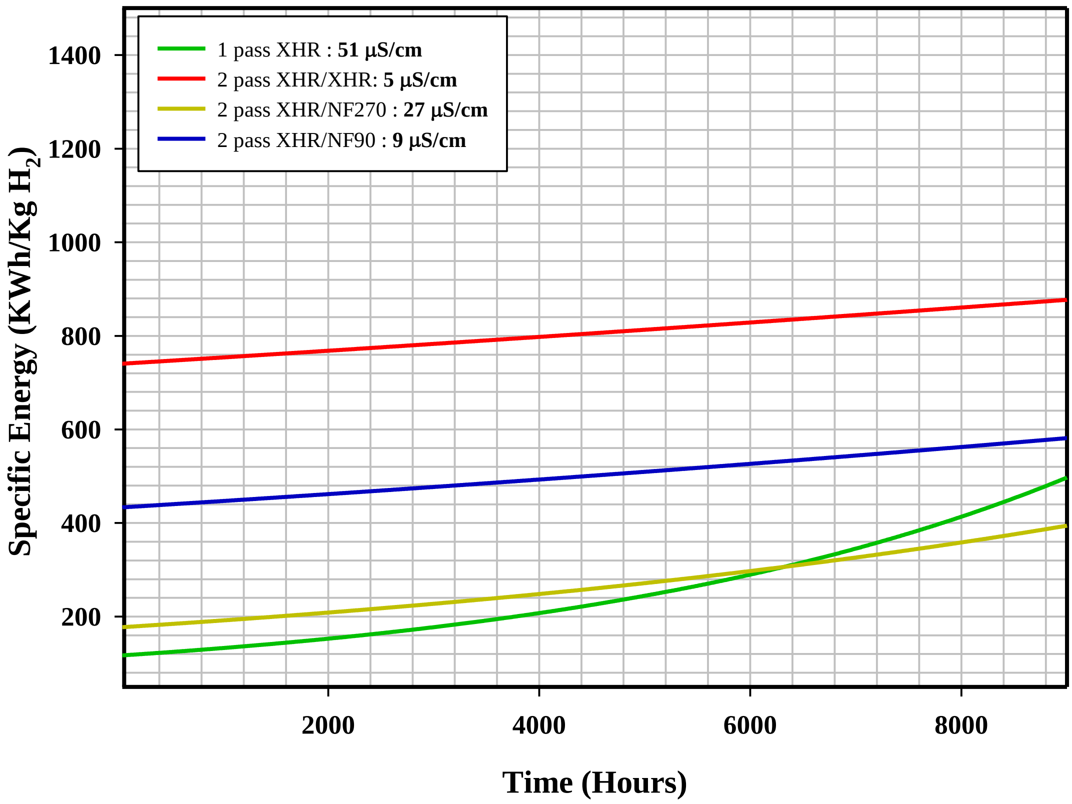

Figure V.11: Specific energy vs. time: configuration effect for Lias water permeate

Figure V.12 presents the corresponding energy efficiency trends. The single-pass XHR system starts with the highest efficiency due to moderate conductivity (51 µS/cm), but this quickly deteriorates. The double-pass XHR/XHR configuration (5 µS/cm), while offering excellent purity, suffers from low and constant efficiency, highlighting the drawbacks of ultra-pure water. The double-pass XHR/NF systems (27 and 9 µS/cm) provide better stability in performance, with the 9 µS/cm configuration emerging as the most balanced in terms of efficiency retention over time.

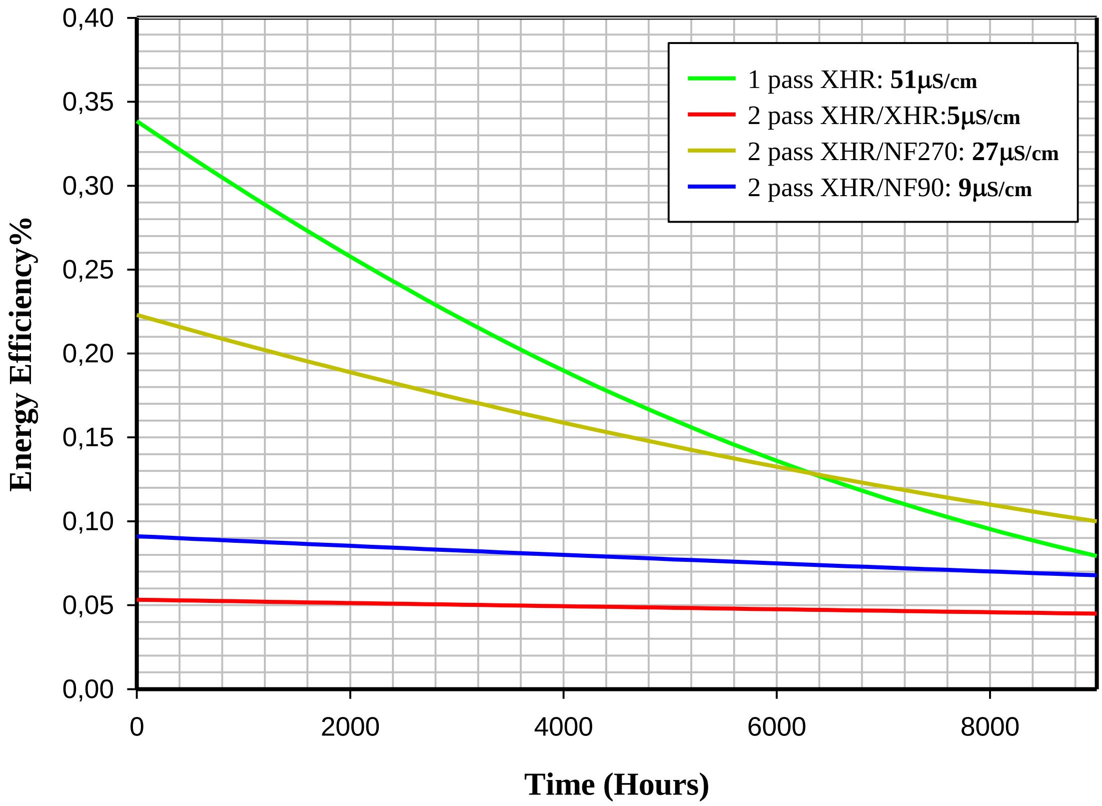

Figure V.12: Energy efficiency vs. Time for different membranes and unit configuration: Lias water

V. 3.3 Case of Albian water permeate

Figure V.13 shows the influence of membrane choice on specific energy consumption when treating Albian water. The XLE 440i membrane (112 µS/cm) starts with a lower energy demand but exhibits rapid degradation. Conversely, the BW30XHR-Pro 440i membrane (30 µS/cm) maintains the lowest and most stable energy consumption throughout the operation. Although some membranes appear more efficient initially, they deteriorate faster, leading to higher cumulative energy demand. The BW30XHR-Pro 440i offers the best long-term behavior and is therefore recommended for Albian water treatment in hydrogen production.

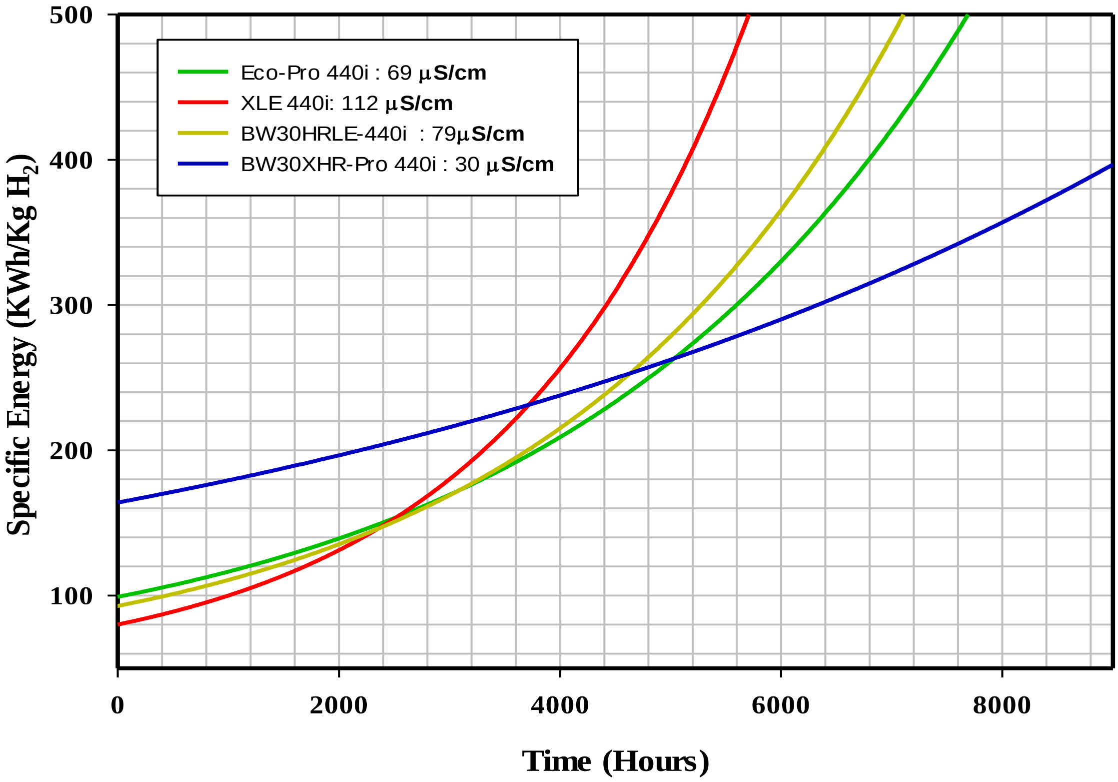

Figure V.13: Specific energy vs. time: Membrane type effect for Albian water permeate

Figure V.14 presents the effect of different treatment configurations on energy consumption over time. Systems delivering lower purity (e.g., single-pass XHR) start with favorable energy metrics but degrade more rapidly. Ultra-pure configurations such as double-pass XHR/XHR (6 µS/cm) are more stable but consistently energy-intensive. Hybrid systems like XHR/NF-90 strike the best compromise, providing both acceptable energy consumption and stable operation over time. The double-pass XHR/NF-90 configuration stands out as the most optimal for sustained hydrogen production from Albian water.

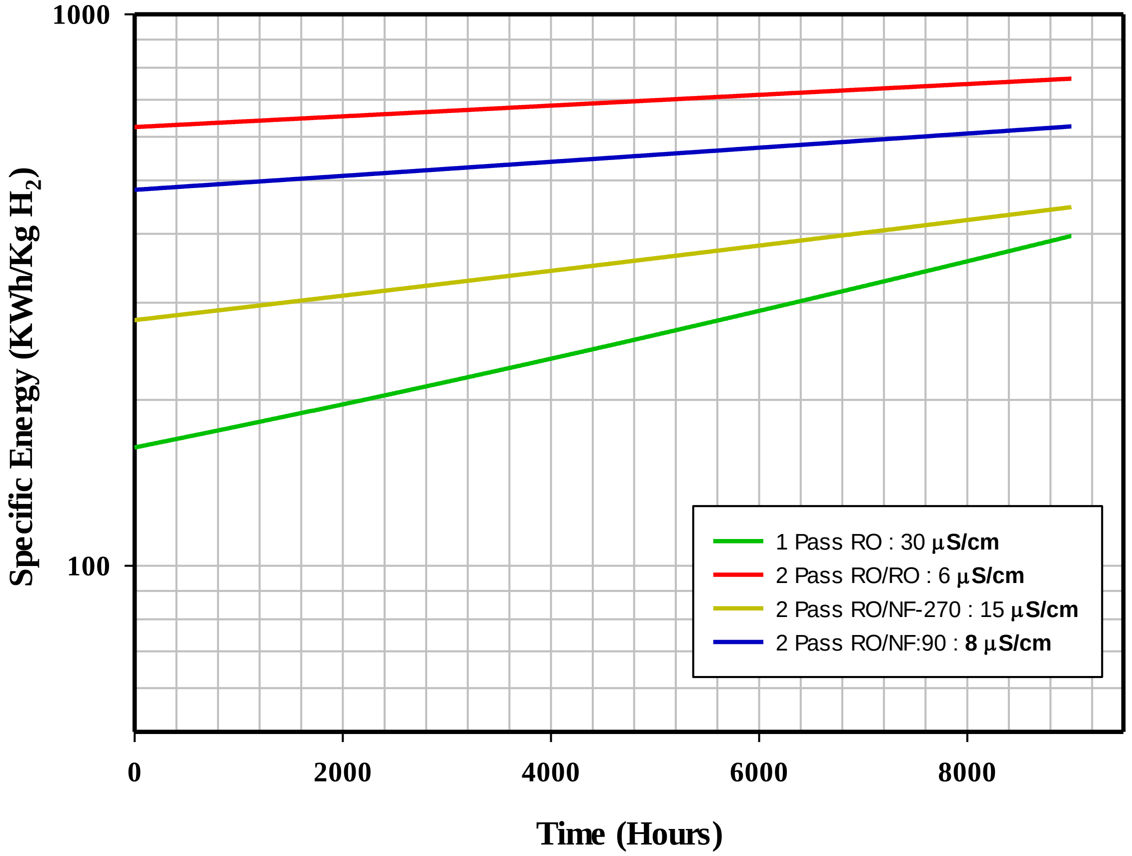

Figure V.14: Specific energy vs. time: configuration effect for Albian water permeate

Figure V.15 tracks the decline in energy efficiency over time for the same configurations. The single-pass XHR configuration (30 µS/cm) initially achieves the highest efficiency but rapidly declines. In contrast, systems with greater water purity, such as XHR/XHR (6 µS/cm) and XHR/NF90 (8 µS/cm), maintain more stable, albeit lower, efficiency throughout. Among these, the XHR/NF-90 configuration shows the least steep efficiency decline**,** which confirms its superior durability. These results illustrate the classic trade-off between initial performance and long-term operational resilience.

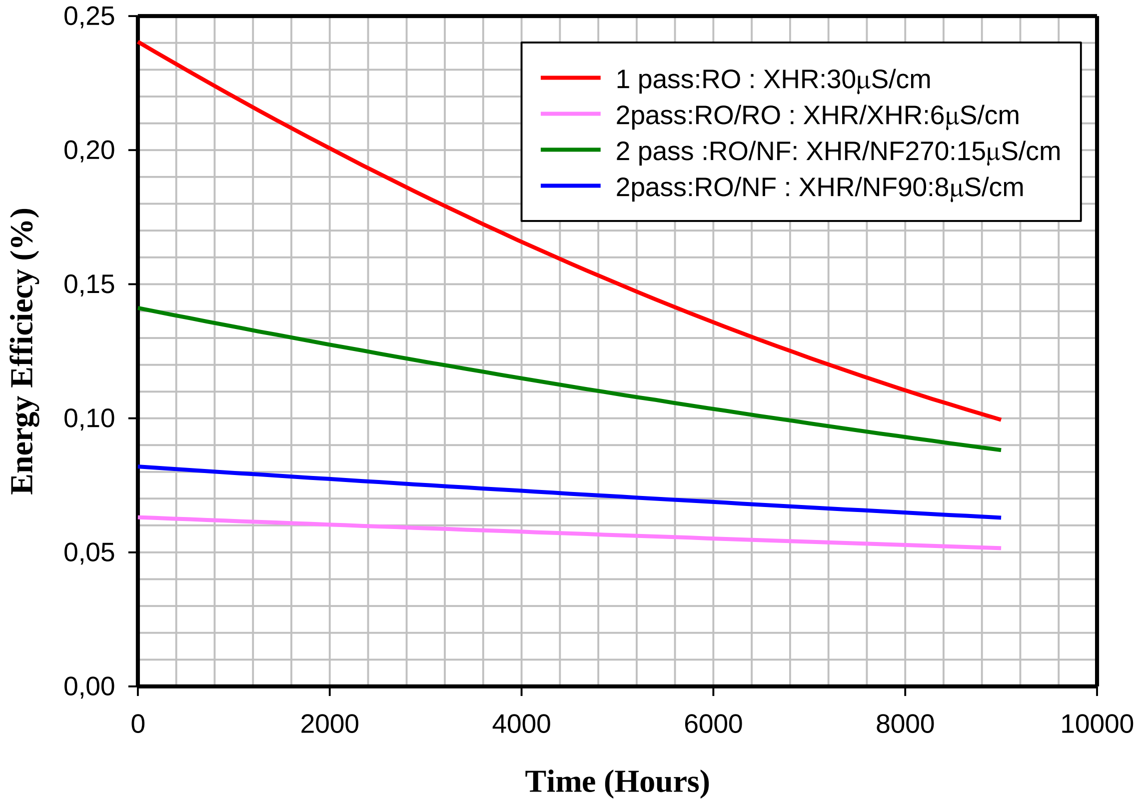

Figure V.15: Energy efficiency vs. Time for different membranes and unit configuration: Albian water

V. 4 Water Resources comparison

This final section presents a comparative analysis of the three water resources studied: seawater, Lias (brackish) water, and Albian (deep groundwater) water. For consistency and fairness, only the most optimal treatment configuration identified for each resource (typically a double-pass RO/NF system) has been considered. This allows for a direct and meaningful comparison of how the origin and conductivity of feedwater influence the performance of a PEM electrolyzer.

The comparison focuses on two key performance indicators over time: specific energy consumption (kWh/kg H_2) and energy efficiency (%). These indicators reflect not only the initial quality of the treated water but also how this quality affects the degradation behavior of the PEM system during prolonged operation. The results provide valuable insights into the trade-offs between water purity, conductivity, and long-term electrolyzer performance, helping to identify the most suitable water source for sustainable hydrogen production.

Figure V.16 compares specific energy consumption over time for the most optimal treatment configurations applied to different water sources, all using double-pass RO/NF systems. Seawater (35 µS/cm) starts with the lowest energy consumption but shows a steady increase due to progressive degradation. Lias water (9 mS/cm) has a slightly higher initial energy demand but maintains a much more controlled curve over time. Albian water (8 µS/cm) requires the most energy from the outset but remains the most stable over time. These results demonstrate that while high conductivity sources are more efficient initially, they accelerate system wear.

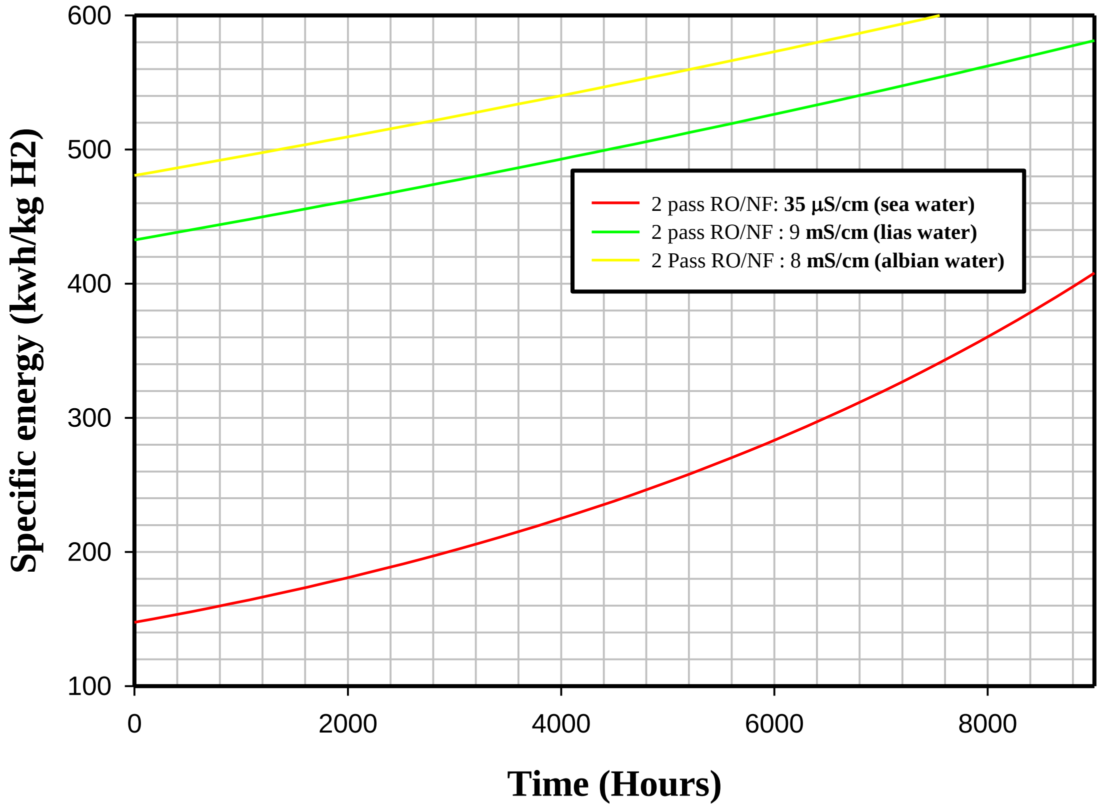

Figure V.16: Specific energy consumption vs. time for different water sources permeate

Figure V.17 presents energy efficiency evolution under the same conditions. Seawater starts with the highest simulated efficiency (~0.27%) but deteriorates quickly. Lias water shows moderate performance and a more gradual reduction in efficiency. Albian water, despite the lowest efficiency (~0.07%), maintains this performance steadily over time. These trends indicate that although high-conductivity feed waters promote higher initial performance, moderate conductivity offers better durability, and ultra-low conductivity preserves long-term stability at the cost of efficiency.

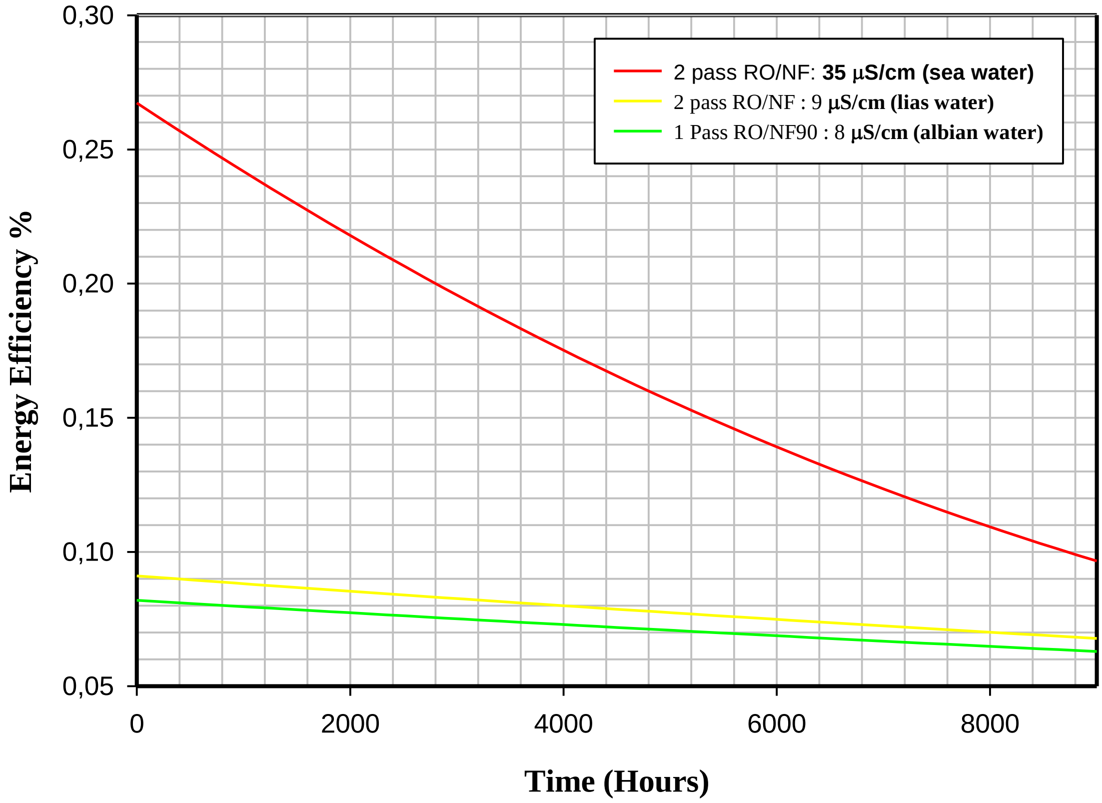

Figure V.17: Energy efficiency (%) Vs. time for hydrogen production using different water sources permeate

The comparative analysis between the three investigated water sources (seawater, Lias water, and Albian water treated using the most optimal configurations selected in each case (primarily double-pass RO/NF systems), highlights several key findings regarding the energy performance and durability of PEM electrolyzers.

Seawater, after treatment resulting in a permeate with a conductivity of 35 µS/cm, demonstrated the highest initial energy efficiency. However, this performance deteriorated rapidly over time, which is likely due to the continued presence of moderate ionic content that accelerates membrane degradation. Although energy consumption was initially low, the long-term sustainability of this configuration proved to be limited.

Lias water, with a conductivity of 9 µS/cm after treatment, offered a more balanced and stable behavior. While its initial efficiency was slightly lower than that of seawater, the system maintained a more gradual and controlled increase in energy consumption over time. This configuration thus represents the most favorable compromise between water quality, energy performance, and system longevity.

In contrast, Albian water, characterized by a very low conductivity (8 µS/cm), led to higher initial energy consumption and the lowest energy efficiency overall. Nevertheless, this performance remained remarkably stable throughout the simulation period. These results suggest that while very pure water limits degradation, it also reduces the electrochemical conductivity necessary for optimal electrolyzer operation, resulting in diminished efficiency from the outset.

Overall, this comparison reveals a fundamental trade-off between water purity and system performance. Higher purity ensures long-term stability but may hinder efficiency, while moderate conductivity can enhance performance initially but leads to quicker degradation. Among the three cases, Lias water treated with a double-pass RO/NF configuration clearly emerges as the most balanced and optimal solution for efficient and durable hydrogen production via PEM electrolysis.

General conclusion

General conclusion and Future Perspectives

This study has clearly demonstrated the critical influence of water quality on the energy performance and long-term durability of PEM electrolyzers, through a combined simulation approach using WAVE for water treatment modeling and Simulink for dynamic electrolysis simulation. The WAVE simulations showed that double-pass hybrid configurations, particularly RO/NF90, offer the best trade-off between low residual conductivity and moderate specific energy consumption across the three water sources analyzed: seawater, Lias, and Albian aquifers. These treated water profiles were then used as inputs for the Simulink-based PEM model to assess their effects on internal resistance, specific energy consumption, and electrolyzer efficiency over time.

The results reveal that while treated seawater initially provides high energy efficiency, it leads to rapid performance degradation due to its relatively higher remaining ionic content. On the other hand, Albian water, characterized by very low conductivity, ensures stable operation but suffers from low initial efficiency due to limited ionic transport. Lias water emerges as the most balanced option, offering a favorable compromise between initial performance, system longevity, and energy consumption, making it the most suitable for sustained hydrogen production.

Looking ahead, this integrated approach opens promising avenues for future research. A multi-objective optimization framework could be developed to dynamically select the best water treatment configurations based on electrolyzer operating conditions. Furthermore, experimental validation of the simulation results is essential, particularly by incorporating membrane fouling dynamics, local polarization effects, and preventive maintenance strategies. Extending the analysis to other membrane types, alternative reverse osmosis architectures, and different electrolyzer technologies (such as AEM or alkaline) would further enhance the general applicability and industrial relevance of the findings, particularly in water-scarce regions such as Algeria.

Reference

[1] République démocratique populaire d'Algérie, "Algeria's National Hydrogen Development Strategy," 2023, [Online]. Available: https://www.energy.gov.dz/?article=stratgie-nationale-de-dveloppement-de-l-hydrogne-en-algrie-4

[2] S. Shiva Kumar and H. Lim, "An overviofwaterelectrolysistechnologiesforgreenhydrogen production," *Energy Reports*, vol. 8, pp. 13793–13813, 2022, doi: 10.1016/j.egyr.2022.10.127.

[3] N. Armaroli and V. Balzani, "The hydrogen issue," *ChemSusChem*, vol. 4, no. 1, pp. 21–36, 2011, doi: 10.1002/cssc.201000182.

[4] P. P. Edwards, V. L. Kuznetsov, and W. I. F. David, "Hydrogen energy," *Philos. Trans. R. Soc. A Math. Phys. Eng. Sci.*, vol. 365, no. 1853, pp. 1043–1056, 2007, doi: 10.1098/rsta.2006.1965.

[5] "Hydrogen power is gaining momentum, but critics say it's neither efficient nor green enough." [Online]. Available: https://www.cnbc.com/2022/01/06/what-is-green-hydrogen-vs-blue-hydrogen-and-why-it-matters.html

[6] A. K. Coker, *Hydrogen Production and Purification*. 2018. doi: 10.1002/9781119257110.ch11.

[7] A. Chirosca and E. Rusu, "Green Hydrogen — Production and Storage Methods : Current Status and Future Directions," 2024.

[8] "The Colors of Hydrogen .Hydrogen Europe." [Online]. Available: https://hydrogeneurope.eu/in-a-nutshell/

[9] J. M. M. Arcos and D. M. F. Santos, "The Hydrogen Color Spectrum: Techno-Economic Analysis of the Available Technologies for Hydrogen Production," *Gases*, vol. 3, no. 1, pp. 25–46, 2023, doi: 10.3390/gases3010002.

[10] R. Adolph, "GREEN HYDROGEN CHARACTERISATION INITIATIVES: DEFINITIONS, STANDARDS, GUARANTEES OF ORIGIN, AND CHALLENGES," pp. 1–23, 2016.

[11] M. A. Rosen and S. Koohi-Fayegh, "The prospects for hydrogen as an energy carrier: an

overview of hydrogen energy and hydrogen energy systems," *Energy, Ecol. Environ.*, vol. 1, no. 1, pp. 10–29, 2016, doi: 10.1007/s40974-016-0005-z.

[12] A. S. S.A. Sherif, D. Yogi Goswami, E.K. (Lee) Stefanakos, *Handbook of Hydrogen Energy*. [Online]. Available: https://books.google.dz/books?id=jGkLBAAAQBAJ&lpg=PP1&ots=DIDi1wg6HC&dq=Introduction to hydrogen energy&lr&hl=fr&pg=PR6#v=onepage&q&f=false

[13] R. Ameta, M. S. Solanki, S. Benjamin, and S. C. Ameta, *Photocatalysis*. 2018. doi: 10.1016/B978-0-12-810499-6.00006-1.

[14] A. A. Levikhin and Boryaev, "Physical properties and thermodynamic characteristics of hydrogen," *Heliyon*, vol. 10, no. 17, p. e36414, 2024, doi: 10.1016/j.heliyon.2024.e36414.

[15] J. Parra-restrepo, "Caractérisation des hétérogénéités de fonctionnement et de dégradation au sein d ' un électrolyseur à membrane échangeuse de protons (PEM) To cite this version : HAL Id : tel-02942062 soutenance et mis à disposition de l ' ensemble de la Contact : ddoc-," 2020.

[16] Karunia, "ETUDE COMPARATIVE DES REGLEMENTATIONS, GUIDES ET NORMES CONCERNANT LES ELECTROLYSEURS ET LE STOCKAGE D'HYDROGENE," vol. 4, no. June, p. 2016, 2016.

[17] M. R. Rahimpour, M. A. Makarem, and P. Kiani, *Hydrogen Production from Renewable Resources and Wastes*. 2024. doi: 10.1201/9781003382270.

[18] A. Beainy, N. Karami, and N. Moubayed, "Simulink model for a PEM electrolyzer based on an equivalent electrical circuit," *2014 Int. Conf. Renew. Energies Dev. Countries, REDEC 2014*, pp. 145–149, 2014, doi: 10.1109/REDEC.2014.7038547.

[19] M. S. Ummah, *Electrochemical water electrolysis fundamentals and technologies*, vol. 11, no. 1. 2019. [Online]. Available: http://scioteca.caf.com/bitstream/handle/123456789/1091/RED2017-Eng-8ene.pdf?sequence=12&isAllowed=y%0Ahttp://dx.doi.org/10.1016/j.regsciurbeco.2008.06.005%0Ahttps://www.researchgate.net/publication/305320484_SISTEM_PEMBETUNGAN_TERPUSAT_STRATEGI_MELESTARI

[20] M. Carmo, D. L. Fritz, J. Mergel, and D. Stolten, "A comprehensive review on PEM water electrolysis," *Int. J. Hydrogen Energy*, vol. 38, no. 12, pp. 4901–4934, 2013, doi: 10.1016/j.ijhydene.2013.01.151.

[21] J. A. Dodwell, “Electrocatalyst Degradation in Polymer Electrolyte Membrane Water Electrolysers”.

[22] S. Dokhani, M. Assadi, and B. G. Pollet, “Techno-economic assessment of hydrogen production from seawater,” *Int. J. Hydrogen Energy*, vol. 48, no. 26, pp. 9592–9608, 2023, doi: 10.1016/j.ijhydene.2022.11.200.

[23] A. Majumdar, M. Haas, I. Elliot, and S. Nazari, “Control and control-oriented modeling of PEM water electrolyzers: A review,” *Int. J. Hydrogen Energy*, vol. 48, no. 79, pp. 30621–30641, 2023, doi: 10.1016/j.ijhydene.2023.04.204.

[24] P. Patel and K. Ayers, *Electrolysis for hydrogen production*, vol. 44, no. 9. 2019. doi: 10.1557/mrs.2019.210.

[25] Z. Abdin, C. J. Webb, and E. M. Gray, “Modelling and simulation of a proton exchange membrane (PEM) electrolyser cell,” *Int. J. Hydrogen Energy*, vol. 40, no. 39, pp. 13243–13257, 2015, doi: 10.1016/j.ijhydene.2015.07.129.

[26] A. Bazarah *et al.*, “Factors influencing the performance and durability of polymer electrolyte membrane water electrolyzer: A review,” *Int. J. Hydrogen Energy*, vol. 47, no. 85, pp. 35976–35989, 2022, doi: 10.1016/j.ijhydene.2022.08.180.

[27] H. A. L. Id, “Étude expérimentale d ’ une cellule d ’ électrolyseur à membrane échangeuse de protons (PEMWE) : contribution à l ’ optimisation d ’ une Pile A Combustible Réversible (PAC-R), pour le stockage d ’ énergie solaire Sébastien Boulevard To cite this versi,” 2021.

[28] M. El-Shafie, “Hydrogen production by water electrolysis technologies: A review,” *Results Eng.*, vol. 20, no. September, p. 101426, 2023, doi: 10.1016/j.rineng.2023.101426.

[29] P. Olivier, C. Bourasseau, and P. B. Bouamama, “Low-temperature electrolysis system modelling: A review,” *Renew. Sustain. Energy Rev.*, vol. 78, no. February, pp. 280–300, 2017, doi: 10.1016/j.rser.2017.03.099.

[30] B. Han, S. M. Steen, J. Mo, and F. Y. Zhang, “Electrochemical performance modeling of a proton exchange membrane electrolyzer cell for hydrogen energy,” *Int. J. Hydrogen Energy*, vol. 40, no. 22, pp. 7006–7016, 2015, doi: 10.1016/j.ijhydene.2015.03.164.

[31] N. Z. Dmitri Bessarabov, Haijiang Wang, Hui Li, *PEM Electrolysis for Hydrogen Production, Principles and Applications. Chapter 11: Degradation Processes and Failure*

Mechanisms in PEM Water Electrolyzers, no. 9. 2016.

[32] M. E. Lebbal and S. Lecœuche, "Identification and monitoring of a PEM electrolyser based on dynamical modelling," *Int. J. Hydrogen Energy*, vol. 34, no. 14, pp. 5992–5999, 2009, doi: 10.1016/j.ijhydene.2009.02.003.

[33] R. Escobar-Yonoff, D. Maestre-Cambronel, S. Charry, A. Rincón-Montenegro, and I. Portnoy, "Performance assessment and economic perspectives of integrated PEM fuel cell and PEM electrolyzer for electric power generation," *Heliyon*, vol. 7, no. 3, 2021, doi: 10.1016/j.heliyon.2021.e06506.

[34] P. Choi, D. G. Bessarabov, and R. Datta, "A simple model for solid polymer electrolyte (SPE) water electrolysis," *Solid State Ionics*, vol. 175, no. 1–4, pp. 535–539, 2004, doi: 10.1016/j.ssi.2004.01.076.

[35] M. G. Santarelli, M. F. Torchio, and P. Cochis, "Parameters estimation of a PEM fuel cell polarization curve and analysis of their behavior with temperature," *J. Power Sources*, vol. 159, no. 2, pp. 824–835, 2006, doi: 10.1016/j.jpowsour.2005.11.099.

[36] Á. Hernández-Gómez, V. Ramirez, and D. Guilbert, "Investigation of PEM electrolyzer modeling: Electrical domain, efficiency, and specific energy consumption," *Int. J. Hydrogen Energy*, vol. 45, no. 29, pp. 14625–14639, 2020, doi: 10.1016/j.ijhydene.2020.03.195.

[37] P. Fragiacomo and M. Genovese, "Modeling and energy demand analysis of a scalable green hydrogen production system," *Int. J. Hydrogen Energy*, vol. 44, no. 57, pp. 30237–30255, 2019, doi: 10.1016/j.ijhydene.2019.09.186.

[38] P. Gabrielli, B. Flamm, A. Eichler, M. Gazzani, J. Lygeros, and M. Mazzotti, "Modeling for optimal operation of PEM fuel cells and electrolyzers," *EEEIC 2016 - Int. Conf. Environ. Electr. Eng.*, 2016, doi: 10.1109/EEEIC.2016.7555707.

[39] H. Zhang, S. Su, G. Lin, and J. Chen, "Efficiency calculation and configuration design of a PEM electrolyzer system for hydrogen production," *Int. J. Electrochem. Sci.*, vol. 7, no. 5, pp. 4143–4157, 2012, doi: 10.1016/s1452-3981(23)19527-7.

[40] R. García-Valverde, N. Espinosa, and A. Urbina, "Simple PEM water electrolyser model and experimental validation," *Int. J. Hydrogen Energy*, vol. 37, no. 2, pp. 1927–1938, 2012, doi: 10.1016/j.ijhydene.2011.09.027.

[41] A. M. I. Noor Azam *et al.*, "Parametric Study and Electrocatalyst of Polymer Electrolyte Membrane (PEM) Electrolysis Performance," *Polymers (Basel.*, vol. 15, no. 3, 2023, doi: 10.3390/polym15030560.

[42] IRENA, *Reduction Hydrogen*. 2020.

[43] N. A. Kelly, *Hydrogen production by water electrolysis*. 2014. doi: 10.1533/9780857097736.2.159.

[44] R. Patel, T. S. Bhatti, and D. P. Kothari, "MATLAB/Simulink-based transient stability analysis of a multimachine power system," *Int. J. Electr. Eng. Educ.*, vol. 39, no. 4, pp. 320–336, 2002, doi: 10.7227/IJEEE.39.4.3.

[45] "Version of Record: https://www.sciencedirect.com/science/article/pii/S1773224724000935," 2024.

[46] V. Ruuskanen, J. Koponen, K. Huoman, A. Kosonen, M. Niemelä, and J. Ahola, "PEM water electrolyzer model for a power-hardware-in-loop simulator," *Int. J. Hydrogen Energy*, vol. 42, no. 16, pp. 10775–10784, 2017, doi: 10.1016/j.ijhydene.2017.03.046.

[47] M. Koundi *et al.*, "Investigation of Hydrogen Production System-Based PEM EL: PEM EL Modeling, DC/DC Power Converter, and Controller Design Approaches," *Clean Technol.*, vol. 5, no. 2, pp. 531–568, 2023, doi: 10.3390/cleantechnol5020028.

[48] A. H. A. Rahim, A. S. Tijani, F. H. Shukri, S. Hanapi, and K. I. Sainan, "Mathematical modelling and simulation analysis of PEM electrolyzer system for hydrogen production," *IET Semin. Dig.*, vol. 2014, no. CP659, 2014, doi: 10.1049/cp.2014.1466.

[49] F. J. Folgado, I. González, and A. J. Calderón, "Simulation platform for the assessment of PEM electrolyzer models oriented to implement digital Replicas," *Energy Convers. Manag.*, vol. 267, no. June, 2022, doi: 10.1016/j.enconman.2022.115917.

[50] D. Yasser *et al.*, "Modélisation dynamique et du vieillissement des PEMFCs dans les applications de mobilité lourde To cite this version : HAL Id : hal-04180872 Modélisation dynamique et du vieillissement des PEMFCs dans les applications de mobilité lourde," 2023.

[51] M. Keddar, M. Da Conceicao, M. L. Doumbia, and Z. Zhang, "Electrolyzer Degradation-Power Electronics One-Way Interaction Model," *Energy Proc.*, vol. 25, 2022, doi: 10.46855/energy-proceedings-9968.

[52] Ö. F. Selamet, F. Becerikli, M. D. Mat, and Y. Kaplan, “Development and testing of a highly efficient proton exchange membrane (PEM) electrolyzer stack,” *Int. J. Hydrogen Energy*, vol. 36, no. 17, pp. 11480–11487, 2011, doi: 10.1016/j.ijhydene.2011.01.129.